Article

Cell Chemical Biology

Identification of covalent inhibitors that disrupt *M. tuberculosis* growth by targeting multiple serine hydrolases involved in lipid metabolism

Graphical abstract

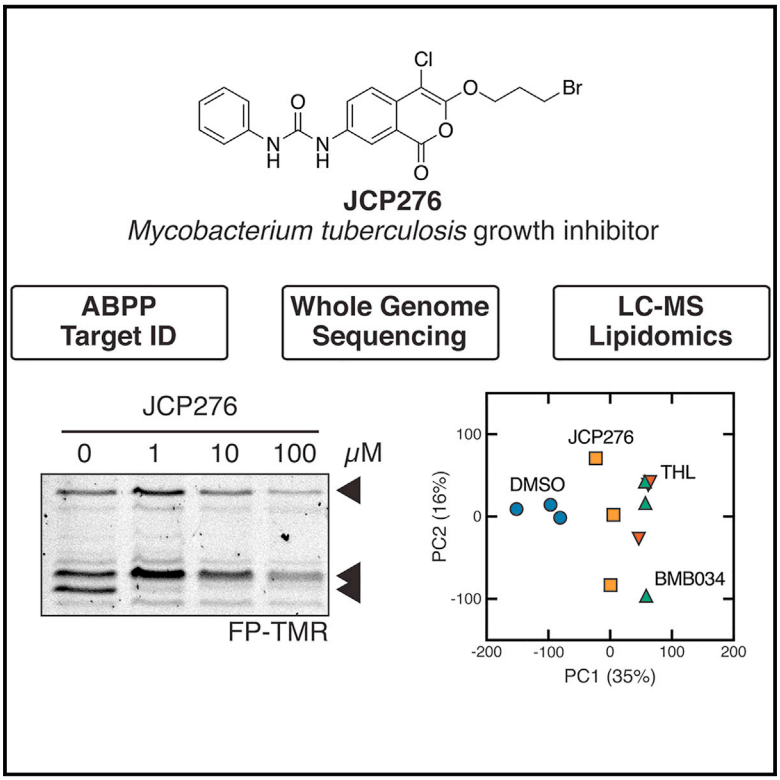

Authors

Brett M. Babin, Laura J. Keller, Yishay Pinto, ..., Ami S. Bhatt, Jonathan Z. Long, Matthew Bogyo

Correspondence

mbogyo@stanford.edu

In brief

The increasing incidence of drug-resistant *Mycobacterium tuberculosis* necessitates the discovery of new therapeutics and therapeutic targets. Babin et al. use a phenotypic screen to identify a potent covalent inhibitor of *M. tuberculosis* growth that targets serine hydrolases and disrupts lipid metabolism.

Highlights

- JCP276 is a narrow-spectrum inhibitor of *Mycobacterium tuberculosis* growth
- Phthiocerol dimycocerate confers resistance to JCP276
- JCP276 inhibits multiple nonessential serine hydrolases
- Serine hydrolase inhibitors lead to an accumulation of free fatty acids

Babin et al., 2022, Cell Chemical Biology *29*, 897–909
May 19, 2022
https://doi.org/10.1016/j.chembiol.2021.08.013

CellPress

Cell Chemical Biology

CellPress

Article

Identification of covalent inhibitors that disrupt *M. tuberculosis* growth by targeting multiple serine hydrolases involved in lipid metabolism

Brett M. Babin,[1] Laura J. Keller,[2] Yishay Pinto,[3,4] Veronica L. Li,[5] Andrew S. Eneim,[1,8] Summer E. Vance,[4] Stephanie M. Terrell,[1] Ami S. Bhatt,[3,4] Jonathan Z. Long,[1,6] and Matthew Bogyo[1,7,9,*]

[1]Department of Pathology, Stanford University School of Medicine, Stanford, CA 94305, USA
[2]Department of Chemical and Systems Biology, Stanford University School of Medicine, Stanford, CA 94305, USA
[3]Department of Genetics, Stanford University School of Medicine, Stanford, CA 94305, USA
[4]Divisions of Hematology and Blood & Marrow Transplantation, Department of Medicine, Stanford University School of Medicine, Stanford, CA 94305, USA
[5]Department of Chemistry, Stanford University, Stanford, CA 94305, USA
[6]Stanford ChEM-H, Stanford University, Stanford, CA 94305, USA
[7]Department of Microbiology & Immunology, Stanford University School of Medicine, Stanford, CA 94305, USA
[8]Present address: Department of Biophysics and Biophysical Chemistry, Johns Hopkins University School of Medicine, Baltimore, MD 21205, USA
[9]Lead contact
*Correspondence: mbogyo@stanford.edu
https://doi.org/10.1016/j.chembiol.2021.08.013

SUMMARY

The increasing incidence of antibiotic-resistant *Mycobacterium tuberculosis* infections is a global health threat necessitating the development of new antibiotics. Serine hydrolases (SHs) are a promising class of targets because of their importance for the synthesis of the mycobacterial cell envelope. We screen a library of small molecules containing serine-reactive electrophiles and identify narrow-spectrum inhibitors of *M. tuberculosis* growth. Using these lead molecules, we perform competitive activity-based protein profiling and identify multiple SH targets, including enzymes with uncharacterized functions. Lipidomic analyses of compound-treated cultures reveal an accumulation of free lipids and a substantial decrease in lipooligosaccharides, linking SH inhibition to defects in cell envelope biogenesis. Mutant analysis reveals a path to resistance via the synthesis of mycocerates, but not through mutations to SH targets. Our results suggest that simultaneous inhibition of multiple SH enzymes is likely to be an effective therapeutic strategy for the treatment of *M. tuberculosis* infections.

INTRODUCTION

Tuberculosis is a top 10 cause of death worldwide and the leading cause of death by a bacterial pathogen. The successful treatment of tuberculosis is a challenging, multifaceted problem whose solution will require improvements in diagnostics, antibiotic access, and treatment monitoring. The increasing incidence of antibiotic resistance in the causative agent of tuberculosis, *Mycobacterium tuberculosis*, is a growing global health threat. Identification of new drug targets and new antibiotics that circumvent resistance is an important step in combatting tuberculosis.

Serine hydrolases (SHs) are a promising class of potential therapeutic enzyme targets for new antibiotics. SHs are involved in a variety of critical cellular processes, including lipid homeostasis, metabolism of host lipids, and cell wall synthesis and maintenance (Bachovchin and Cravatt, 2012). Because SHs have many roles in assembly, modification, and maintenance of the extensive mycobacterial cell envelope, they are overrepresented in the *M. tuberculosis* genome compared with other pathogenic bacteria (Cotes et al., 2008). They comprise 4.0% of the proteome (158 of 4,080 total proteins) compared with 2.2%, 1.5%, and 1.9% for the other common bacterial pathogens *Pseudomonas aeruginosa* (133 of 5,888 total proteins), *Salmonella enterica* (67 of 4,533 total proteins), and *Staphylococcus aureus* (49 of 2,583 total proteins) (Lentz et al., 2018), respectively. SHs are also more prevalent in *M. tuberculosis* than in the human proteome (~1.2%, ~240 of more than 20,000 total proteins) (Simon and Cravatt, 2010). Furthermore, many *M. tuberculosis* SHs lack human homologs, suggesting that it is feasible to develop inhibitors that are unreactive toward host enzymes. In addition, small molecules that target human SHs have been developed to treat a range of conditions, including hypertension, obesity, diabetes, and others (Bachovchin and Cravatt, 2012). One of the most successful therapeutic small-molecule SH inhibitors is tetrahydrolipstatin (THL) (marketed as Orlistat), which is used

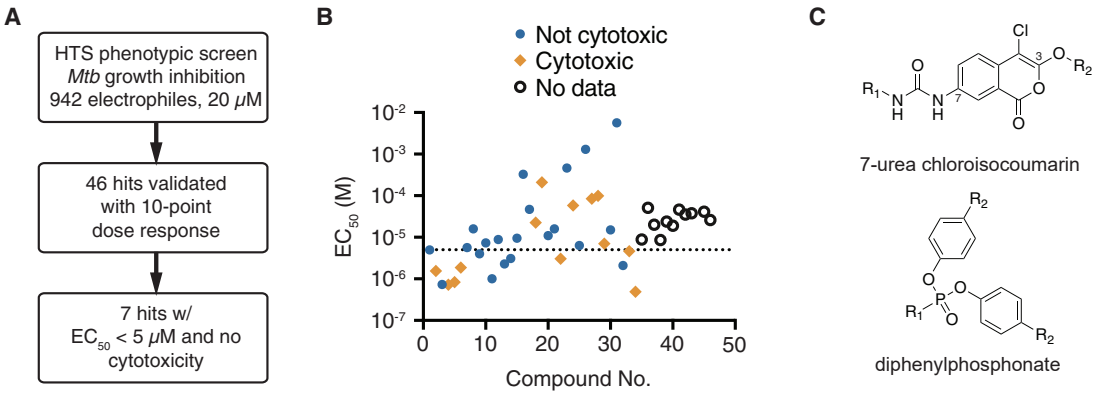

Figure 1. Screen of electrophilic compounds yields inhibitors of *M. tuberculosis* growth

(A) Screening strategy.

(B) EC_{50} values for 46 hits. Cytotoxicity data were obtained from Gruner et al. (2016). The dotted line indicates the 5 μM cutoff used to prioritize hits.

(C) Core scaffolds of the top 7 hits.

See also Tables S1 and S2.

to treat obesity by blocking key lipid mobilizing enzymes in the gut, thus blocking the utilization of dietary fats (Borgstrom, 1988; Drent and van der Veen, 1993). Furthermore, the extensive efforts to develop SH inhibitors as therapeutics have created diverse compound classes that inhibit these enzymes and have established successful strategies to optimize compound selectivity (Adibekian et al., 2011; Bachovchin et al., 2010; Chang et al., 2013; Faucher et al., 2020). Therefore, SHs are a highly diverse and "druggable" family of targets whose function in bacteria remains poorly defined.

Previous studies have identified small-molecule inhibitors of *M. tuberculosis* SHs, including THL (Low et al., 2009), the mammalian liposomal acid lipase inhibitor lalistat (Lehmann et al., 2016), the cyclipostin CyC_{17} (Nguyen et al., 2017), the human hormone-sensitive lipase inhibitor M*m*PPOX (Delorme et al., 2012), the β-lactone EZ120 (Lehmann et al., 2018), and the triazole ureas AA691 and AA692 (Li et al., 2021). These inhibitors all make use of an electrophile that covalently modifies the active site serine present in all members of this enzyme class. While these studies demonstrate the importance of SHs as therapeutic targets, they generally have been unable to determine the mechanism by which SH inhibition interferes with *M. tuberculosis* growth or viability. A key benefit of using inhibitors that covalently modify the active site of their protein targets is that those targets can be readily identified by activity-based protein profiling (ABPP) mass spectrometry (MS) experiments. ABPP experiments have been used to identify targets for each of the SH inhibitors listed (Lehmann et al., 2016, 2018; Li et al., 2021; Ravindran et al., 2014). However, all of the reported SH inhibitors with activity in *M. tuberculosis* target multiple SHs, making it difficult to identify the enzyme or set of enzymes whose functions are essential for bacterial survival. In most cases, the genes that code for SHs are not essential (Griffin et al., 2011; Rengarajan et al., 2005; Sassetti et al., 2003; Sassetti and Rubin, 2003), suggesting that efficacy of bactericidal or bacteriostatic SH inhibitors likely relates to their ability to simultaneously inhibit multiple enzymes.

We sought to perform a phenotypic, cell-based screen of a highly focused library of potential covalent SH inhibitors to identify compounds that inhibit *M. tuberculosis* growth. We reasoned that such a screen would yield hits that could then be used to clarify the mechanisms by which SH inhibition leads to growth inhibition and help to prioritize SHs as potential therapeutic targets. Because the library consists exclusively of covalent binding electrophiles, it was possible to use hit compounds to directly identify targeted SHs. From this screen, we identified a series of 7-urea chloroisocoumarin inhibitors with narrow-spectrum activity toward *M. tuberculosis* that lacked human cell cytotoxicity. We performed competitive ABPP proteomic experiments and identified multiple protein targets covalently modified by this class of compounds, including uncharacterized lipases. We used LC-MS-based lipidomics and whole-genome sequencing of a resistant mutant to demonstrate that these SHs are involved in aspects of lipid biogenesis that are disrupted by inhibitor treatment, thus making them promising therapeutic targets.

RESULTS

High-throughput screening yields electrophilic inhibitors of *M. tuberculosis* growth

We screened a library of 942 compounds featuring cysteine- and serine-reactive electrophiles (Child et al., 2013; Hall et al., 2011) for their ability to inhibit exponential growth of *M. tuberculosis* in culture (Figure 1A). We tested compounds at a single dose (20 μM) with a 1-week incubation, which yielded a 4.9% hit rate (46/942 compounds; Table S1). To validate the 46 hit compounds, we performed a 10-point dose-response analysis to calculate the half-maximal effective concentration (EC_{50}) values (Figure 1B; Table S2). Of the top 14 compounds with EC_{50} < 5 μM, 7 were excluded due to host cell cytotoxicity as reported previously for human pancreatic cell lines (Gruner et al., 2016). The validated hits consisted of two core chemical scaffolds: 7-urea chloroisocoumarins and peptide diphenylphosphonates (Figure 1C; Table 1), both of which are expected to target the active site of SHs or proteases. Although the screening library contains many chloroisocoumarin compounds with diverse substitutions at the 7 position, we note that only those featuring a urea arose as hits.

Table 1. Screening hits

Compound	Class[a]	Structure	EC_{50} (μM)[b]	Mammalian cell growth (%)[c]
JCP276	u-CIC	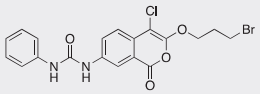	1.7 ± 0.2	112
BMB034	u-CIC	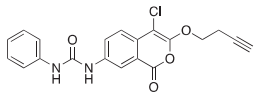	8.7 ± 1.1	N/D
BMB038	u-CIC	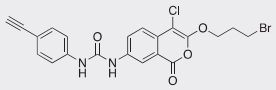	36 ± 11	N/D
JCP089	DPP	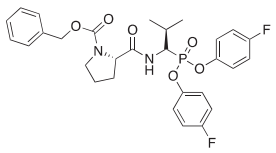	0.72	96
JCP086	u-CIC	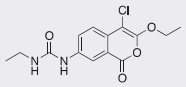	0.73	70
JCP137	DPP	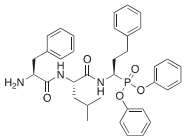	0.84	88
JCP161	u-CIC	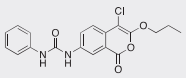	1.0	72
JCP071	DPP	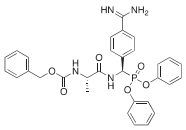	1.6	131
JCP142	DPP	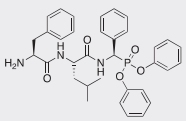	1.9	96
JCP272	u-CIC	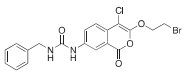	2.1	73
JCP164	u-CIC	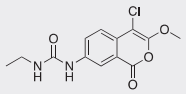	2.3	30
JCP205	u-CIC	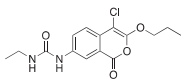	3.0	86
JCP166	u-CIC	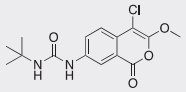	3.1	36
JCP155	u-CIC	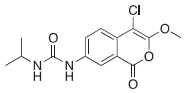	4.0	36

(*Continued on next page*)

Table 1. *Continued*

Compound	Class[a]	Structure	EC_{50} (μM)[b]	Mammalian cell growth (%)[c]
JCP275	u-ClC	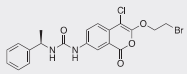	4.7	110
JCP048	DPP	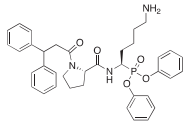	5.0	84

Nontoxic hit compounds are indicated in italics.
[a]u-ClC, 7-urea chloroisocoumarin; DPP, diphenylphosphonate.
[b]EC_{50} values for JCP276, BMB034, and BMB038 are reported as the mean ± standard deviation (n = 3). EC_{50} values for other compounds are reported without error and were calculated from a single dose-response experiment (n = 1).
[c]Cytotoxicity data were obtained from (Gruner et al., 2016). N/D, not determined.

We chose to focus all subsequent efforts on the most potent compound from the validated hits, JCP276 (Figure 2A; Table 1). Upon resynthesis, it showed similar potency for growth inhibition after 1 week of incubation, as observed in the original screen, with an EC_{50} of 1.7 μM and an EC_{90} of 10 μM (Figure 2B). Three-week incubations revealed a minimum inhibitory concentration (MIC) of 50 μM (23 mg/L). Treating liquid cultures with a sub-MIC of JCP276 resulted in growth arrest for approximately 14 days, followed by outgrowth (Figure 2C), suggesting that the activity is bacteriostatic, and that differences in 1- and 3-week potencies may be due to compound degradation. Indeed, growth inhibition could be maintained by a second addition of JCP276 at day 14, suggesting that this effect was a result of compound degradation rather than evolved resistance. We used LC-MS to measure JCP276 stability in growth medium and calculated a half-life of 60 h (Figure S1). With this rate of degradation, we expect the concentration of JCP276 to be below 1 μM after 2 weeks of incubation, consistent with the observed outgrowth.

To evaluate the selectivity of JCP276, we tested its effect on nontuberculous mycobacteria (NTM), other bacteria, and mammalian cells. While JCP276 inhibited growth of our laboratory strain of *M. tuberculosis* (designated BBMT01) and a clinical isolate of *M. kansasii*, the compound had no effect on the growth of *Escherichia coli* or *Staphylococcus aureus* at doses up to 100 μM (Figure 2D). Faster growing mycobacteria and pathogenic NTM isolates *M. smegmatis*, *M. marinum*, *M. intracellulare*, *M. abscessus*, and *M. avium* were similarly unaffected, suggesting a narrow spectrum of activity. JCP276 was also not cytotoxic to a murine macrophage cell line or human foreskin fibroblasts up to 100 μM after 24 h of incubation (Figure 2E).

Phthiocerol dimycocerosate regulates susceptibility to JCP276

We attempted to generate spontaneous resistance mutants by culturing a high concentration of bacteria on solid agar containing supra-MICs of JCP276. We performed initial experiments using 4×10^6 CFU with 100 μM JCP276 but these attempts did not yield any resistant colonies (two independent experiments). However, we were able to isolate resistant clones by increasing the number of cells applied to each plate to 2×10^9 CFU (500-fold more cells). Resistant strains (BBMT04, BBMT05, and BBMT06) were isolated from three different solid cultures. We treated liquid cultures of each strain with JCP276 and confirmed that all three exhibited a shift in EC_{50} values in excess of 100-fold (Figure 3A, $EC_{50} > 300$ μM). Whole-genome sequencing of the starting, non-resistant strain BBMT01 revealed 93 mutations compared with the H37Rv reference genome, including frameshifts and point mutations that resulted in the truncation of seven proteins (Table S3). Many of the mutations (42%) were found in *pe/ppe* genes, known hotspots for sequence variation in the *M. tuberculosis* genome (McEvoy et al., 2012). We chose one resistant mutant, BBMT05, for whole-genome sequencing and found 92 of the 93 mutations identified in the BBMT01. The one exception was a 7-bp insertion in the *ppsA* gene. Unexpectedly, the insertion yielded a gene sequence that exactly matched the reference genome, reverting a frameshift mutation identified in BBMT01. We performed PCR and Sanger sequencing to confirm the mutation and to verify the sequences of this region for the BBMT04 and BBMT06 strains as well. For all three mutants that exhibited resistance to JCP276, we found that the *ppsA* truncation was reverted back to the reference sequence (Figure 3B). This observation suggests that BBMT01 is not isogenic but rather contains a majority of cells that feature the *ppsA* mutation combined with a small subpopulation coding for the full-length gene. This subpopulation with a fully functional *ppsA* gene is less sensitive to JCP276 and therefore became highly enriched in our resistance study. If the *ppsA*-intact subpopulation is present at very low levels, this would also explain our inability to generate resistant mutants when starting with fewer cells in the inoculum.

PpsA is a phenolphthiocerol ketide synthase that serves as part of the PpsABCDE complex required for the synthesis of phthiocerol dimycocerosate (PDIM) (Trivedi et al., 2005). PpsA catalyzes the first steps in the extension and modification of lipids to convert long-chain fatty acids (mycosanoic acids) into mycocerosic acids and phthioceranic acids, which are assembled to make PDIM. The truncated copy of PpsA encoded by BBMT01 lacks the catalytic domains required for lipid processing and for transfer to the next polyketide synthase (PKS) in the assembly line of PDIM synthesis (Figure 3C). Thus, BBMT01 lacks the ability to produce PDIM. Laboratory culture is known to select for *M. tuberculosis* strains that lack PDIM, often via mutation of the *pps* genes, because

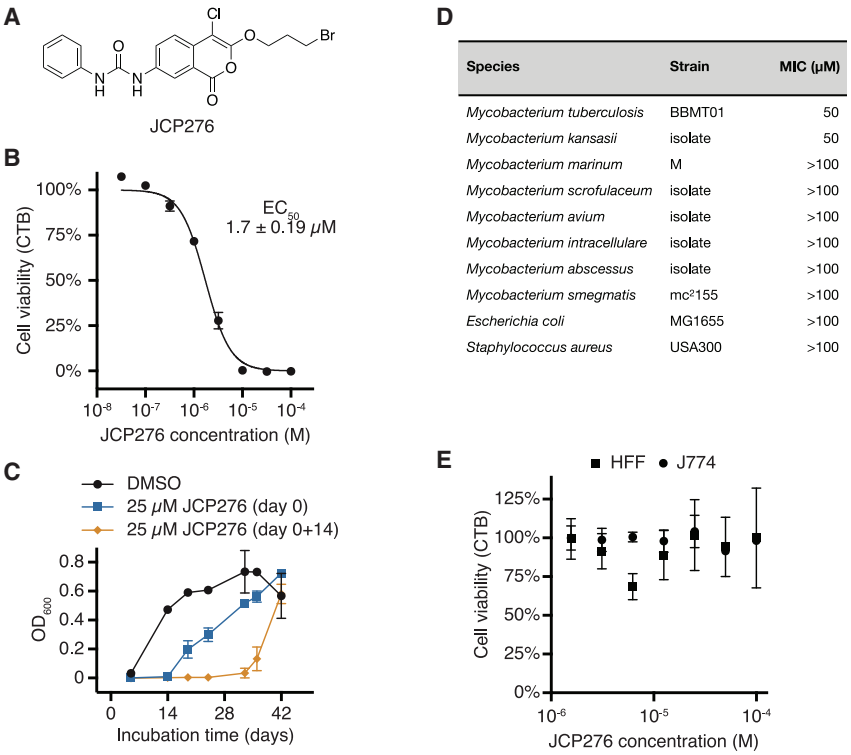

Species	Strain	MIC (μM)
Mycobacterium tuberculosis	BBMT01	50
Mycobacterium kansasii	isolate	50
Mycobacterium marinum	M	>100
Mycobacterium scrofulaceum	isolate	>100
Mycobacterium avium	isolate	>100
Mycobacterium intracellulare	isolate	>100
Mycobacterium abscessus	isolate	>100
Mycobacterium smegmatis	mc²155	>100
Escherichia coli	MG1655	>100
Staphylococcus aureus	USA300	>100

Figure 2. JCP276 is a narrow-spectrum inhibitor of *M. tuberculosis* growth

(A) Structure of JCP276.

(B) Dose-dependent inhibition of *M. tuberculosis* growth by JCP276 following a 7-day incubation. Data represent the mean ± standard deviation of three biological replicates. Data were fit to two-parameter parametric model (solid line) and the EC_{50} is reported as the mean ± 95% confidence interval.

(C) Growth of *M. tuberculosis* as measured by OD_{600}. JCP276 was added at day 0 of the experiment (blue squares) or at day 0 and again at day 14 (orange diamonds). Data represent the mean ± standard deviation of three biological replicates.

(D) MIC_{90} of JCP276 for various bacterial strains as measured by visual inspection of growth in well plates.

(E) Cytotoxicity measurements for mammalian cell lines in the presence of JCP276. Data represent the mean ± standard deviation of three biological replicates.

See also Figure S1.

PDIM-deficient cells have a growth advantage in standard medium (Domenech and Reed, 2009). In addition, PDIM serves as a formidable barrier for small-molecule uptake, and it is well characterized that PDIM-deficient strains are more susceptible to an array of antibiotics (Chavadi et al., 2011; Mohandas et al., 2016). Therefore, we hypothesize that cells deficient in PDIM synthesis readily uptake JCP276, allowing inhibition of growth so that only a small subpopulation of PDIM competent cells can be cultured in the presence of supra-MIC of JCP276.

Based on the genome sequencing data, we considered the possibility that the production of dimycocerosates (DIMs) by a strain or species is the primary feature that determines its susceptibility to JCP276. To test this hypothesis, we evaluated a panel of our mycobacteria for PDIM. Lipids were extracted from BBMT01, BBMT05, and the NTM strains and analyzed by thin-layer chromatography for DIMs. As a control, we used PDIM isolated from *M. marinum.* As expected, BBMT05 produced PDIM but BBMT01 did not (Figure S2A). Analysis of the NTM strains showed that our isolate of *M. kansasii* produces a lipid species with higher polarity than the *M. tuberculosis* PDIM (Figure S2B), likely corresponding to the smaller, phthiodiolone-based DIM produced by that species (Minnikin et al., 2015; Onwueme et al., 2005). It is known that *M. avium* does not produce DIMs (Onwueme et al., 2005) and indeed neither *M. avium* nor the other NTM strains produced detectable DIMs. Based on the observations that *M. kansasii* produces DIMs and is susceptible to JCP276, and that the other NTM strains do not produce DIMs and are not susceptible, we conclude that DIM production by a given species does not determine its susceptibility to JCP276.

ABPP enables the identification of hydrolase targets of JCP276

Because the chloroisocoumarin electrophile is expected to covalently modify the active site of SHs, we used competitive ABPP to identify protein targets of JCP276 and the structurally similar hit JCP275 (EC_{50} = 4.7 μM, Table 1). We used fluorophosphonate (FP) coupled to either biotin or tetramethylrhodamine (TMR) (Figure 4A) as a general probe for SHs. Cells were treated with JCP276 or JCP275 for 1 h and lysates were treated with FP-TMR to label the active site of SHs. Labeled proteins were visualized via SDS-PAGE (Figures 4B and S3A). Five proteins were competed by the inhibitors at doses at or above the EC_{50} values of the two inhibitors, suggesting that both compounds target multiple SHs.

While most SHs are targeted by FP (Bachovchin et al., 2010), we considered the possibility that the chloroisocoumarin electrophile inhibits proteins that are not labeled in the FP competition experiment. To account for this possibility, we synthesized alkyne probe versions of JCP276, featuring the alkyne attached either to the 3 position (BMB034, Figure 4C; Table 1) or the 7 position (BMB038, Table 1) of the chloroisocoumarin core. Both BMB034 and BMB038 inhibited *M. tuberculosis* growth in culture, albeit with decreased potencies compared with the parent compound JCP276, with EC_{50} values of 8.7 and 36 μM, respectively (Figure S3B). We used BMB034 for competitive ABPP because it was the more potent of the two probes. After incubation of live cells in culture with BMB034, we lysed the cells, and performed click chemistry with azide-TMR to visualize BMB034-labeled proteins. A few distinct proteins were consistently labeled by 1 μM BMB034 (Figure 4D), while higher doses (10 and 100 μM) labeled a larger set of proteins (Figure S3C). Pretreatment of cultures with JCP276 at 1 or 10 μM clearly competed for labeling of four proteins by 1 μM BMB034 (Figure 4D). Competition was also observed with 10 μM of BMB034 (Figure S3D), but competed bands were difficult to distinguish from the increase in overall labeling. As a negative

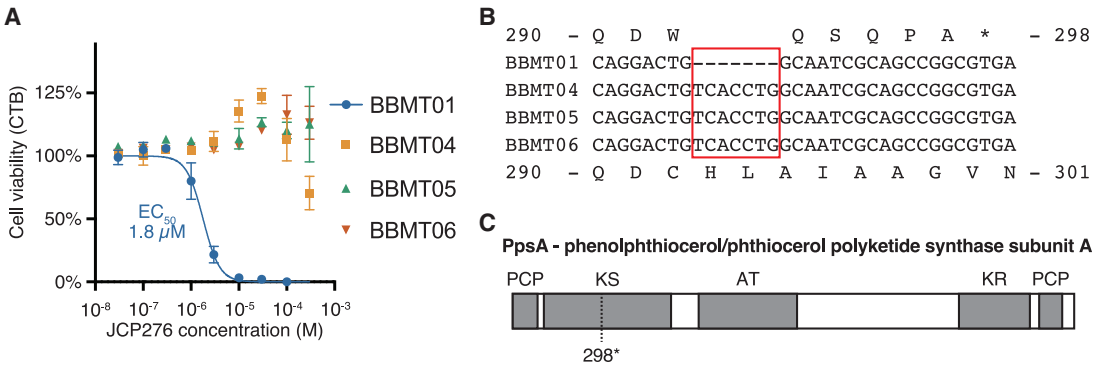

Figure 3. PDIM competency confers resistance to JCP276

(A) Dose-dependent inhibition of wild-type and mutant *M. tuberculosis* growth by JCP276 following a 7-day incubation. Data represent the mean ± standard deviation of three biological replicates. Data were fit to a two-parameter parametric model (solid line).

(B) Sanger sequencing results for the *ppsA* gene. Amino acid sequences are annotated above (BBMT01) and below (others). Amino acids are indicated above or below the first base of each triplet codon.

(C) Diagram of PpsA protein with the location of the premature stop codon at residue 298 indicated. Domains are indicated: PCP, peptidyl carrier protein; KS, β-ketoacyl ACP synthase; AT, acyl transferase; and KR, ketoreductase.

See also Figure S2 and Table S3.

control we pre-treated cells with dichloroisocoumarin (DCI), a general inhibitor of SHs and proteases that does not inhibit *M. tuberculosis* growth, and found that it did not compete with BMB034 labeling (Figures S3D and S3E). These data suggest that BMB034-labeled proteins are likely phenotypically relevant targets of JCP276.

To identify putative JCP276 targets, we used the general SH probe FP-biotin or BMB034 and then performed click labeling with desthiobiotin to affinity purify the labeled proteins for MS analysis. We chose concentrations of JCP276 that resulted in clear competition in our gel-based experiments: 10 and 100 μM for FP competition and 1 and 10 μM for BMB034 competition. For both probes, we pre-treated cells with the lead inhibitor JCP276 and then measured the change in recovery of the target SH proteins. We found that the set of FP-biotin-labeled proteins overlapped substantially with the list of FP-reactive proteins reported in three previous studies, confirming that our probe labeling was working as expected (Li et al., 2021; Ortega et al., 2016; Patel et al., 2018; Tallman et al., 2016) (Table S4). Overall, we identified 25 of the 27 proteins (93%) found in all 3 existing datasets and 44 of the 47 proteins (94%) found in at least 2 existing datasets. These comparisons suggest that, despite differences in probe design, enrichment protocols, and culture conditions, our FP enrichment experiment captured the majority of FP-reactive enzymes. Because protein targets of JCP276 are expected to be depleted in the pre-treatment conditions, we calculated abundance ratios between proteins enriched from cells that had been pre-treated with 10 or 100 μM of JCP276 or JCP275, relative to the DMSO-treated control (Table S4). Abundance ratios for each predicted SH (Tallman et al., 2016) correlated well between both the JCP275 and JCP276 pre-treated samples (n = 55, r = 0.87, Figure S4A), suggesting that each compound inhibits the same set of protein targets with similar potencies and likely acts via the same mechanism. Nine of the 55 identified proteins were significantly reduced in abundance by 10 μM pre-treatment with JCP276 (Figure 4E) or JCP275 (Figure S4B). The abundance ratios were the same or lower following pre-treatment with 100 μM of each compound, confirming the expected dose response of true targets.

Enrichment via BMB034 yielded a smaller set of predicted SHs. While the entire enrichment experiment yielded 106 protein identifications, only 7 were competed by pre-treatment with 10 μM JCP276, and only 4 of those were not competed by DCI (Table S4). These 4 proteins are all predicted SHs that were identified as putative targets in the FP enrichment experiment (Figure 4E). Five of the proteins competed in the FP enrichment experiment were not detected in the BMB034 enrichment experiment, suggesting potential differences in the target binding properties of the alkyne probe BMB034 compared with the original JCP276 lead molecule. The concentration of BMB034 used in direct labeling experiments (1 μM) was below its EC_{50} so it is possible that some target proteins were not sufficiently labeled at this lower dose and therefore were not identified in the direct labeling study. A large number of the identified proteins were not competed by JCP276 and are not annotated as SHs, suggesting that they are likely artifacts of the enrichment procedure.

Taken together, the two enrichment experiments define a set of nine putative protein targets that includes predicted esterases and lipases (e.g., LipO, LipI, LipG, NlhH/LipH), although neither the biochemical activity nor the biological function of most of these putative targets have been confirmed. Importantly, none of the genes encoding the putative targets are annotated as essential according to transposon-sequencing datasets (Griffin et al., 2011; Rengarajan et al., 2005; Sassetti et al., 2003; Sassetti and Rubin, 2003). The fact that inhibition of each target individually is not expected to cause a growth defect suggests that JCP276 acts by simultaneous inhibition of multiple SH targets.

Lipidomic analysis links THL and chloroisocoumarin mechanisms of growth inhibition

It is currently unclear how polypharmacological inhibition of SHs disrupts bacterial growth. Because many of the protein targets of JCP276 and other SH inhibitors are biochemically and biologically uncharacterized, target identification alone is insufficient

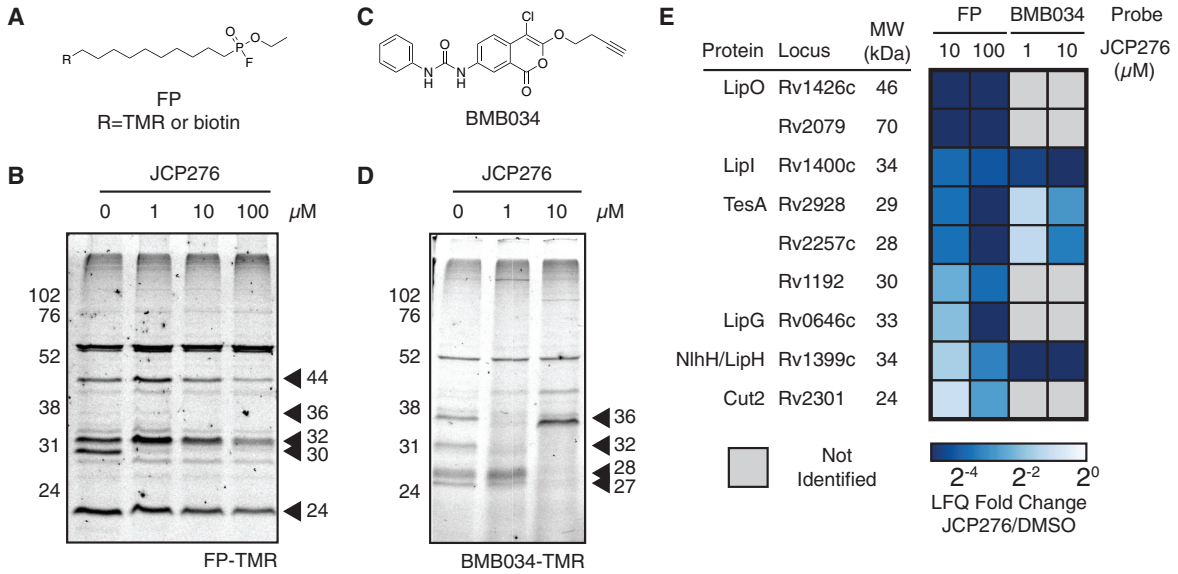

Figure 4. ABPP reveals serine hydrolase targets of JCP276

(A) Structure of FP probe.

(B) Competitive ABPP using FP-TMR. Bacterial cultures were treated with DMSO or JCP276 as indicated for 1 h at 37°C. Labeling was performed in lysates by treatment of lysed cells with 1 μM FP-TMR for 30 min at 37°C. Proteins were separated by SDS-PAGE and gels scanned for TMR fluorescence using a flatbed scanner.

(C) Structure of BMB034 probe.

(D) Competitive ABPP using BMB034. Bacterial cultures were pre-treated with DMSO, JCP276, or DCI as indicated for 1 h at 37°C. Labeling was performed in intact cells by treatment of live cells with 1 μM BMB034 for 1 h at 37°C. Cells were then lysed and subjected to click chemistry conditions with azide-TMR. Proteins were separated by SDS-PAGE and gels scanned for TMR fluorescence using a flatbed scanner.

(E) Summary of proteomic results from FP and BMB034 ABPP experiments. The heatmap represents the ratio of the abundance of each protein between cultures treated with JCP276 at the indicated doses and cultures treated with DMSO.

See also Figures S3 and S4 and Table S4.

to develop a model for a mechanism of action. Because many of the putative targets are expected to be involved in the synthesis and modification of lipids, we hypothesized that inhibitor treatment might alter cellular lipid profiles. To compare the modes of action between the chloroisocoumarin inhibitors and a previously reported lipase inhibitor, we compared lipid profiles from cells treated with JCP276, BMB034, or THL at twice their MICs. We extracted lipids from bacterial cultures and performed an analysis using LC-MS. The resulting spectra were annotated by matching ions to the MycoMass database (Layre et al., 2011) to identify validated, *Mycobacterium*-specific lipids. Fold changes for each identified lipid were calculated as the ratio of mean integrated ion currents from treated and untreated samples. Across all 4 conditions, we identified and matched 1,206 lipids to the database. Principal-component analysis of individual samples resulted in two clusters: one containing the DMSO-treated control samples, and another containing all of the compound-treated samples (Figure 5A). In addition, treated and untreated samples are differentiated by the first principal component, which explains 35% of the variance among the samples. Results from this analysis suggest that the lipidomic data are consistent among replicates because each treatment condition is separated by PC1 and PC2. It also confirms that bacteria treated with JCP276, BMB034, or THL exhibit a shift in lipid profiles. Finally, it shows that treatment with any of the three compounds results in a similar perturbation to the lipid profiles. The latter observation supports the hypothesis that both chloroisocoumarins and THL act via a similar general mechanism.

To more carefully define the changes in lipid components upon inhibition of SHs, we calculated the mean fold change in ion intensities of compound-treated samples compared with the DMSO-treated controls (Table S5). A global analysis of changes showed strong correlations between JCP276 versus BMB034 ($r = 0.90$) and JCP276 versus THL ($r = 0.89$) (Figures S3A and S3B), further supporting the hypothesis that THL and chloroisocoumarin compounds act via similar lipid perturbations. Although fold changes for individual lipid species varied, the majority of classes had median fold changes that were close to 1 (Figure S5C), suggesting that perturbations were limited to a small subset of lipid classes. The lipid classes that showed the greatest changes were lipooligosaccharides and cardiolipins, which were depleted in compound-treated cells, and the free mycobacterial lipids mycocerosic, phthioceranic, and phthienoic acids, which were enriched (Figures 5B and 5C).

Diverse SH inhibitors target multiple enzymes to disrupt bacterial growth

Given that none of the identified protein targets are encoded by essential genes, we hypothesize that JCP276 acts by targeting multiple SHs whose combined inhibition prevents bacterial growth. This hypothesis is supported by the fact that the

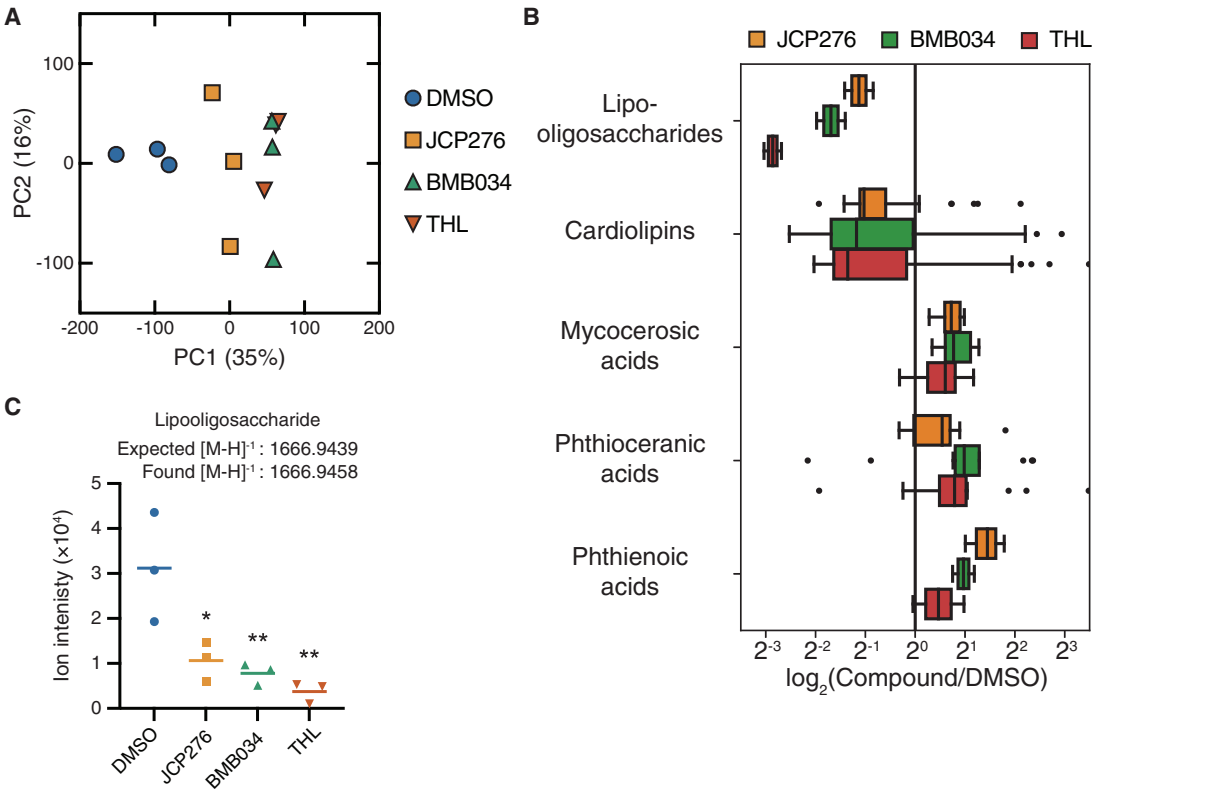

Figure 5. Serine hydrolase inhibitors alter cellular lipid profiles

(A) Principal-component analysis (PCA) of lipid abundances from three biological replicates for each compound treatment. Solid cultures were treated with DMSO or 100 μM of JCP276, BMB034, or THL for 5 days at 37°C. Lipids were extracted and analyzed by LC-MS.

(B) Boxplots of lipid abundance ratios between cultures treated with each compound or cultures treated with DMSO. The vertical line represents the median value for each lipid class, boxes represent the upper and lower quartiles, whiskers represent 1.5 times the interquartile range, and circles represent outliers from this range.

(C) Ion intensities for lipooligosaccharide for each treatment condition. Data from treated cultures were compared with the DMSO control by ANOVA followed by Dunnett's test for multiple comparisons.

See also Figure S5 and Table S5.

previously reported SH inhibitors with anti-mycobacterial activity also target multiple serine hydrolases. We sought to compare the protein targets of this set of compounds to distinguish between targets expected to be important for the cellular effects and targets whose inhibition is not necessary for growth inhibition. We compared the targets of JCP276, THL, lalistat, CyC_{17}, AA692, and EZ120 (Figure 6A), which have been identified in this study and in prior ABPP experiments. Of the 77 predicted SHs in *M. tuberculosis* (Tallman et al., 2016), 40 were identified as targets of at least 1 of the 6 compounds. We note that variations in the design of the ABPP experiments, the probes used, bacterial growth conditions, and LC-MS/MS instruments may result in bona fide targets being missed in any single study. In addition, some protein targets may be more susceptible to small-molecule electrophiles (e.g., those with broad substrate promiscuity, high expression levels, or especially reactive active sites). Because Li et al. (2021) included a structurally similar but less potent compound in their ABPP study, their set of prioritized AA692 targets excludes SHs that are readily targeted by serine-reactive electrophiles but that do not contribute to growth inhibition. Therefore, to narrow down this list of possible targets we sought proteins that are: (1) targeted by at least three of the compounds, (2) targeted by JCP276, (3) targeted by AA692, and (4) not targeted by the less potent triazole urea, AA702 (Li et al., 2021). Of the nine proteins targeted by more than three compounds, only TesA meets these criteria (Figure 6B). LipM, LipN, and Rv1730c are potentially important targets, but we can exclude their role in the activity of JCP276 because they were identified but not competed in our FP ABPP experiment (Table S4). Because TesA is nonessential for growth in culture, it unlikely to be the only target by which JCP276 and the other SH inhibitors exert their effects on mycobacterial growth. However, the above analysis suggests that TesA is an important and shared target of most SH inhibitors, and that growth inhibition may require targeting of TesA along with other lipases.

Given that JCP276 has narrow-spectrum activity against *M. tuberculosis* and *M. kansasii*, we hypothesized that conservation of putative targets among mycobacteria may also explain the differences in susceptibility among bacteria. We performed BLAST analysis of all 77 predicted SHs in *M. tuberculosis* to search for homologs in *M. kansasii* and the non-tubercular mycobacteria whose growth is not inhibited by JCP276. A majority of

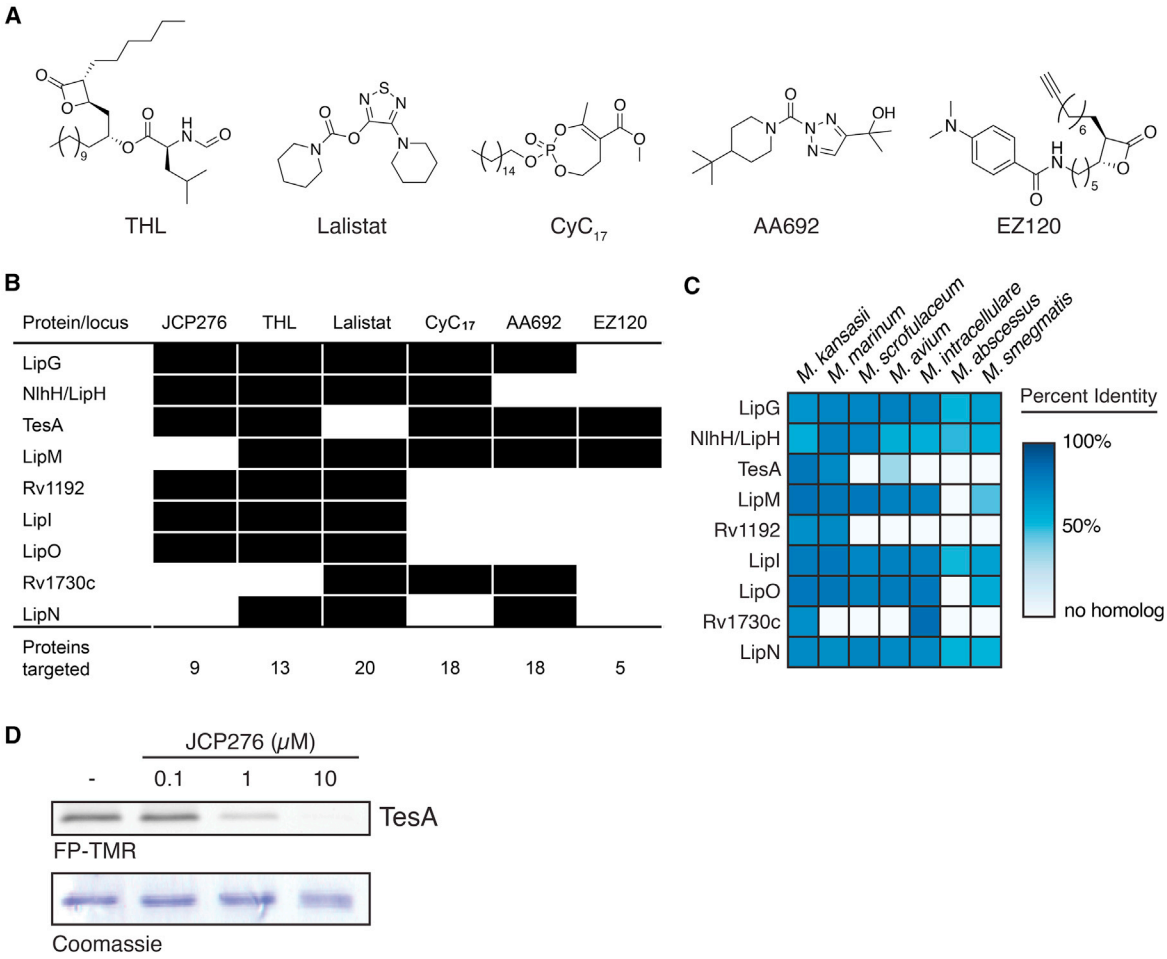

Figure 6. SH inhibitors target a conserved set of enzymes

(A) Structures of SH inhibitors with activity against mycobacteria.

(B) Proteins targeted by at least three of the SH inhibitors from (A) as determined by ABPP. Black boxes indicate that a protein was identified as a target.

(C) Homologs of each protein from (B) in various NTMs. The heatmap indicates the percent identity of each protein to its *M. tuberculosis* homolog. White boxes indicate no homolog in that species.

(D) Competitive ABPP of *M. tuberculosis* TesA. Recombinant TesA was incubated with DMSO or JCP276 as indicated, treated with FP-TMR, and separated by SDS-PAGE. Coomassie stain indicates equal protein loading.

SHs (73%) from *M. tuberculosis* had homologs in all other mycobacteria. Of the targets of JCP276, TesA and Rv1192 are notable because their homologs are present in *M. kansasii* but few other mycobacteria (Figure 6C). In addition, we performed the same BLAST analysis against the human proteome using the same criteria and found no matches, further emphasizing that, despite a substantial number of SHs in humans, future drug development efforts are likely to yield inhibitors of *M. tuberculosis* growth that do not target human enzymes.

Analysis of both the composition of shared SH inhibitor targets and homology across species indicates TesA as a protein that is likely to be important to the inhibitory action of JCP276. To verify that TesA is indeed inhibited by JCP276, we expressed and purified recombinant TesA, pre-treated the enzyme with JCP276, and labeled the active site with FP-TMR (Figure 6D). We observed a dose-dependent decrease in FP labeling consistent with covalent modification of the active site by JCP276, confirming TesA as a target. We also note that overexpression of TesA in *M. bovis* modestly reduced the susceptibility of that organism to THL (Ravindran et al., 2014). Given that treatment with JCP276 and BMB034 induce similar lipidome remodeling as THL, it is likely that the mechanisms of action of each compound are related.

DISCUSSION

This study and others reporting the use of SH inhibitors to disrupt *M. tuberculosis* growth highlight the benefits of a polypharmacological strategy for tuberculosis therapy. In each study, phenotypic screens yielded inhibitors that target multiple enzymes, which, by themselves, are nonessential for growth in culture. Because each target is nonessential, a target-based approach would not have progressed to the development of SH inhibitors. One of the key benefits of antimicrobial compounds that inhibit multiple targets is that there appears to be a larger barrier to evolving resistance. No resistance was observed for the triazole

urea SH inhibitors AA691 and AA692, with resistance rates expected to be lower than 1×10^{-9} (Li et al., 2021). In our study, resistance mutants were obtained at a rate $\sim 2 \times 10^{-9}$, but we note that the mechanism of resistance is likely related to the increased barrier of entry in the mutant strains due to their PDIM production. The fact that PDIM prevents growth inhibition by JCP276 means that this compound is not likely to be a viable antibiotic, given that PDIM is critical for infection (Cox et al., 1999) and that clinical isolates of *M. tuberculosis* are PDIM competent (Domenech and Reed, 2009). However, it is important to note that resistance was not observed via mutation of any of the protein targets of the compound, suggesting that an optimized compound with enhanced cell penetrance would likely not readily yield resistant mutants.

Determining the mechanism of action by which an inhibitor with multiple targets impacts fitness is challenging. Targets whose inhibition is important for growth inhibition can, in principle, be distinguished from other targets by combinatorial genetic knockdown or deletion experiments. However, in the case of SH inhibitors with ~10–20 targets, a full genetic analysis with all combinations is prohibitive. In this study, we used a comparative lipidomic approach in an effort to identify the pathways that are perturbed by JCP276 treatment. Linking the lipidomic results to the inhibition of enzyme activities remains challenging because many of the protein targets in *M. tuberculosis* are biochemically and physiologically uncharacterized. However, the substantial lipid changes upon treatment with SH inhibitors point to a plausible model mechanism in which inhibition of thioesterases leads to a buildup of fatty acids and prevents the synthesis of critical membrane components. It also identifies a signature of lipid accumulation that correlates with bactericidal activity, suggesting that this accumulation could be used as a readout in future drug screens to enable the identification of compounds with multi-target modes of action.

We observe that SH inhibitor treatment results in an accumulation of mycobacterial fatty acids, including mycocerosic, phthioceranic, and phthienoic acids (Figure 5B). *M. tuberculosis* uses a suite of PKSs for the biosynthesis of these complex mycobacterial lipids (Minnikin et al., 2002; Natarajan et al., 2008). A key step in the synthesis of these lipids is the cleavage of the thioester bond which links a given fatty acid to a cysteine residue on its cognate PKS. For example, PDIM synthesis relies on the thioesterase activity of TesA to release lipids produced by the PKSs, PpsABCDE and Mas (Nguyen et al., 2018). In the absence of active thioesterases, fatty acids cannot be removed from PKSs and are therefore not substrates for conjugation to the diverse lipid species, including lipooligosaccharides and cardiolipins, both of which we find to be depleted upon compound treatment. These results are consistent with previous findings regarding SH inhibitor mechanisms. Recent results using a microscopy-based morphological analysis, MorphEUS (Li et al., 2021), concluded that the SH inhibitors AA692 and THL are likely to interfere with cell wall synthesis. In contrast, a different study found that the β-lactone EZ120 caused a decrease in the synthesis of mycolic acids, presumably through its inhibition of Ag85 (Lehmann et al., 2018). In our data, Ag85 is competed by JCP276 but surprisingly not by the structurally similar JCP275, and Ag85 is not enriched by BMB034 (Table S4), suggesting that Ag85 may not be the most important target for growth inhibition by the chloroisocoumarins. In further support of this, we did not observe a decrease in mycolic acids upon treatment with JCP276 (Figure S3C; Table S5).

Although TesA is nonessential for growth in culture, it remains an intriguing target because of its importance for pathogenesis and antibiotic susceptibility. TesA is a virulence factor due to its necessity for the synthesis of PDIM. In addition, *tesA* mutants show increased susceptibility to antibiotics (Bellerose et al., 2020; Chavadi et al., 2011; Yang et al., 2020), presumably due to the increased permeability of PDIM-deficient cells. Indeed, THL treatment increases susceptibility of *M. bovis* to vancomycin via modulation of lipid content (Rens et al., 2016). The fact that BBMT01 contains a mutation in *ppsA* is serendipitous because it allows us to decouple the effects of TesA and other SH inhibition from the increased sensitivity due to PDIM deficiency. In the case of JCP276 activity, it shows that growth inhibition is not related to the role TesA plays in synthesizing PDIM. However, thioesterase activity is important for the synthesis of other lipids as well. While TesA has been characterized for its role in releasing fatty acids from the PpsABCDE and Mas PKS system required for PDIM synthesis, it is not known whether it interacts with other PKS systems. In addition, while the targets of JCP276 are mostly uncharacterized, it has been shown that the lipase LipG also has thioesterase activity (Santucci et al., 2018).

This study highlights the value of utilizing phenotypic, target-agnostic screens to identify new pathways that are susceptible to chemical inhibition for the treatment of *M. tuberculosis*. Our lipidomic data and meta-analyses of prior SH inhibitors point to a polypharmacological mechanism of action in which simultaneous inhibition of key SHs prevents bacterial growth. Future screening efforts would benefit from exploring lipid perturbations in addition to growth inhibition as phenotypic outputs. The diversity of SH inhibitors with anti-mycobacterial activity, and the evidence that targeting multiple SHs may prevent the evolution of resistance, suggests that SHs are potentially important antibiotic targets for *M. tuberculosis*. Furthermore, future efforts in identifying anti-mycobacterial compounds would likely benefit from targeting a critical set of enzymes that have been prioritized through phenotypic screens and functional studies of their roles in lipid metabolism.

SIGNIFICANCE

Tuberculosis (TB) is a top 10 cause of death worldwide. The increasing incidence of antibiotic resistance by the causative agent, the bacterium *Mycobacterium tuberculosis*, is a substantial setback in the battle against TB. Here, we use a screen of covalent, small-molecule inhibitors to identify JCP276, a narrow-spectrum inhibitor of *M. tuberculosis* growth. We identify a set of nonessential serine hydrolase targets of the compound, whose simultaneous inhibition causes growth arrest. Using lipidomic analysis, we show that serine hydrolase inhibitors substantially disrupt the free fatty acid pool. This work demonstrates the value of targeting multiple nonessential enzymes for the generation of new antibiotics.

STAR★METHODS

Detailed methods are provided in the online version of this paper and include the following:

- KEY RESOURCES TABLE
- RESOURCE AVAILABILITY
  - Lead contact
  - Materials availability
  - Data and code availability
- EXPERIMENTAL MODEL AND SUBJECT DETAILS
  - Mycobacterial culture
  - Bacterial culture for recombinant protein expression
  - Mammalian cell culture
- METHOD DETAILS
  - High-throughput screening, hit validation, and EC_{50} determination
  - Growth inhibition measurements
  - MIC measurements
  - Mammalian cell cytotoxicity measurements
  - Compound stability measurements
  - Generation of resistant mutants
  - Whole genome and sanger sequencing of mutants
  - Variant calling
  - PDIM analysis by TLC
  - ABPP labeling and enrichment
  - Proteomic analysis
  - Proteomic data analysis
  - Lipid extraction
  - Lipidomic analysis
  - Lipidomic data analysis
  - Analysis of SH homologs
  - Purification and FP competition of recombinant TesA
  - Chemical synthesis
- QUANTIFICATION AND STATISTICAL ANALYSIS

SUPPLEMENTAL INFORMATION

Supplemental information can be found online at https://doi.org/10.1016/j.chembiol.2021.08.013.

ACKNOWLEDGMENTS

We thank Renier Van der Westhuyzen (Drug Discovery and Development Center, University of Cape Town, South Africa) for assistance with the original phenotypic screen. Mycobacterial clinical isolates were kindly provided by Dr. Nikki Parrish and Derek Armstrong (Department of Pathology, the Johns Hopkins University School of Medicine). We thank Carolyn Bertozzi (Stanford University) for use of the BSL3 facility and mass spectrometry instruments. We thank Nick Riley (Stanford University) and Marc Driessen (Stanford University) for help with mass spectrometry. We thank C.J. Cambier (Stanford University) for providing purified PDIM. We thank Jessica Seeliger (Stony Brook University) for helpful discussions and critical feedback. B.M.B. was supported by the A.P. Giannini Foundation. L.J.K. was supported by the Stanford ChEM-H Chemistry/Biology Interface Predoctoral Training Program, Stanford Molecular Pharmacology Training Grant, and a Stanford Graduate Fellowship. A.S.B. was supported by the Alfred P. Sloan Foundation. This work was also funded in part by grants from the National Institutes of Health (T32AI07328 to B.M.B., T32GM113854 to V.L.L., R01AI148623 to A.S.B., R01DK124265 to J.Z.L., R01AI143757 to A.S.B., R01EB005011 to M.B., and R01EB026332 to M.B.). The content is solely the responsibility of the authors and does not necessarily represent the official views of the National Institutes of Health.

AUTHOR CONTRIBUTIONS

Conceptualization, data curation, formal analysis, investigation, software, visualization, writing – original draft, B.M.B.; data curation, formal analysis, investigation, software, L.J.K.; formal analysis, Y.P.; investigation, V.L.L., A.S.E., S.E.V., and S.M.T.; funding acquisition, resources, supervision, A.S.B.; funding acquisition, resources, J.Z.L.; conceptualization, funding acquisition, resources, supervision, writing – review & editing, M.B.

DECLARATION OF INTERESTS

The authors declare no competing interests.

INCLUSION AND DIVERSITY

One or more of the authors of this paper self-identifies as an underrepresented ethnic minority in science. One or more of the authors of this paper received support from a program designed to increase minority representation in science.

Received: June 7, 2021
Revised: July 29, 2021
Accepted: August 26, 2021
Published: September 23, 2021

REFERENCES

Adibekian, A., Martin, B.R., Wang, C., Hsu, K.L., Bachovchin, D.A., Niessen, S., Hoover, H., and Cravatt, B.F. (2011). Click-generated triazole ureas as ultrapotent in vivo-active serine hydrolase inhibitors. Nat. Chem. Biol. *7*, 469–478.

Bachovchin, D.A., and Cravatt, B.F. (2012). The pharmacological landscape and therapeutic potential of serine hydrolases. Nat. Rev. Drug Discov. *11*, 52–68.

Bachovchin, D.A., Ji, T., Li, W., Simon, G.M., Blankman, J.L., Adibekian, A., Hoover, H., Niessen, S., and Cravatt, B.F. (2010). Superfamily-wide portrait of serine hydrolase inhibition achieved by library-versus-library screening. Proc. Natl. Acad. Sci. U S A *107*, 20941–20946.

Bellerose, M.M., Proulx, M.K., Smith, C.M., Baker, R.E., Ioerger, T.R., and Sassetti, C.M. (2020). Distinct bacterial pathways influence the efficacy of antibiotics against *Mycobacterium tuberculosis*. mSystems *5*, e00396–20.

Borgstrom, B. (1988). Mode of action of tetrahydrolipstatin: a derivative of the naturally occurring lipase inhibitor lipstatin. Biochim. Biophys. Acta *962*, 308–316.

Chang, J.W., Cognetta, A.B., 3rd, Niphakis, M.J., and Cravatt, B.F. (2013). Proteome-wide reactivity profiling identifies diverse carbamate chemotypes tuned for serine hydrolase inhibition. ACS Chem. Biol. *8*, 1590–1599.

Chavadi, S.S., Edupuganti, U.R., Vergnolle, O., Fatima, I., Singh, S.M., Soll, C.E., and Quadri, L.E. (2011). Inactivation of tesA reduces cell wall lipid production and increases drug susceptibility in mycobacteria. J. Biol. Chem. *286*, 24616–24625.

Child, M.A., Hall, C.I., Beck, J.R., Ofori, L.O., Albrow, V.E., Garland, M., Bowyer, P.W., Bradley, P.J., Powers, J.C., Boothroyd, J.C., et al. (2013). Small-molecule inhibition of a depalmitoylase enhances *Toxoplasma* host-cell invasion. Nat. Chem. Biol. *9*, 651–656.

Cotes, K., Bakala N'goma, J.,C., Dhouib, R., Douchet, I., Maurin, D., Carriere, F., and Canaan, S. (2008). Lipolytic enzymes in *Mycobacterium tuberculosis*. Appl. Microbiol. Biotechnol. *78*, 741–749.

Cox, J., and Mann, M. (2008). MaxQuant enables high peptide identification rates, individualized p.p.b.-range mass accuracies and proteome-wide protein quantification. Nat. Biotechnol. *26*, 1367–1372.

Cox, J.S., Chen, B., McNeil, M., and Jacobs, W.R., Jr. (1999). Complex lipid determines tissue-specific replication of *Mycobacterium tuberculosis* in mice. Nature *402*, 79–83.

Danecek, P., Bonfield, J.K., Liddle, J., Marshall, J., Ohan, V., Pollard, M.O., Whitwham, A., Keane, T., McCarthy, S.A., and Davies, R.M. (2021). Twelve years of SAMtools and BCFtools. Gigascience *10*, giab008.

Delorme, V., Diomande, S.V., Dedieu, L., Cavalier, J.F., Carriere, F., Kremer, L., Leclaire, J., Fotiadu, F., and Canaan, S. (2012). MmPPOX inhibits *Mycobacterium tuberculosis* lipolytic enzymes belonging to the hormone-sensitive lipase family and alters mycobacterial growth. PLoS One *7*, e46493.

Domenech, P., and Reed, M.B. (2009). Rapid and spontaneous loss of phthiocerol dimycocerosate (PDIM) from *Mycobacterium tuberculosis* grown in vitro: implications for virulence studies. Microbiology (Reading) *155*, 3532–3543.

Drent, M.L., and van der Veen, E.A. (1993). Lipase inhibition: a novel concept in the treatment of obesity. Int. J. Obes. Relat. Metab. Disord. *17*, 241–244.

Faucher, F., Bennett, J.M., Bogyo, M., and Lovell, S. (2020). Strategies for tuning the selectivity of chemical probes that target serine hydrolases. Cell Chem. Biol. *27*, 937–952.

Garrison, E., and Marth, G. (2012). Haplotype-based Variant Detection from Short-Read Sequencing (arXiv), p. 12073907.

Gowda, H., Ivanisevic, J., Johnson, C.H., Kurczy, M.E., Benton, H.P., Rinehart, D., Nguyen, T., Ray, J., Kuehl, J., Arevalo, B., et al. (2014). Interactive XCMS online: simplifying advanced metabolomic data processing and subsequent statistical analyses. Anal Chem. *86*, 6931–6939.

Griffin, J.E., Gawronski, J.D., Dejesus, M.A., Ioerger, T.R., Akerley, B.J., and Sassetti, C.M. (2011). High-resolution phenotypic profiling defines genes essential for mycobacterial growth and cholesterol catabolism. PLoS Path *7*, e1002251.

Gruner, B.M., Schulze, C.J., Yang, D., Ogasawara, D., Dix, M.M., Rogers, Z.N., Chuang, C.H., McFarland, C.D., Chiou, S.H., Brown, J.M., et al. (2016). An in vivo multiplexed small-molecule screening platform. Nat. Methods *13*, 883–889.

Haedke, U., Gotz, M., Baer, P., and Verhelst, S.H. (2012). Alkyne derivatives of isocoumarins as clickable activity-based probes for serine proteases. Biorg. Med. Chem. *20*, 633–640.

Hall, C.I., Reese, M.L., Weerapana, E., Child, M.A., Bowyer, P.W., Albrow, V.E., Haraldsen, J.D., Phillips, M.R., Sandoval, E.D., Ward, G.E., et al. (2011). Chemical genetic screen identifies *Toxoplasma* DJ-1 as a regulator of parasite secretion, attachment, and invasion. Proc. Natl. Acad. Sci. U S A *108*, 10568–10573.

Kerrigan, J.E., Oleksyszyn, J., Kam, C.M., Selzler, J., and Powers, J.C. (1995). Mechanism-based isocoumarin inhibitors for human leukocyte elastase. Effect of the 7-amino substituent and 3-alkoxy group in 3-alkoxy-7-amino-4-chloroisocoumarins on inhibitory potency. J. Med. Chem. *38*, 544–552.

Layre, E., Sweet, L., Hong, S., Madigan, C.A., Desjardins, D., Young, D.C., Cheng, T.Y., Annand, J.W., Kim, K., Shamputa, I.C., et al. (2011). A comparative lipidomics platform for chemotaxonomic analysis of *Mycobacterium tuberculosis*. Chem. Biol. *18*, 1537–1549.

Lehmann, J., Cheng, T.Y., Aggarwal, A., Park, A.S., Zeiler, E., Raju, R.M., Akopian, T., Kandror, O., Sacchettini, J.C., Moody, D.B., et al. (2018). An antibacterial beta-lactone kills *Mycobacterium tuberculosis* by disrupting mycolic acid biosynthesis. Angew. Chem. Int. Ed. Engl. *57*, 348–353.

Lehmann, J., Vomacka, J., Esser, K., Nodwell, M., Kolbe, K., Ramer, P., Protzer, U., Reiling, N., and Sieber, S.A. (2016). Human lysosomal acid lipase inhibitor lalistat impairs *Mycobacterium tuberculosis* growth by targeting bacterial hydrolases. Med. Chem. Commun. *7*, 1797–1801.

Lentz, C.S., Sheldon, J.R., Crawford, L.A., Cooper, R., Garland, M., Amieva, M.R., Weerapana, E., Skaar, E.P., and Bogyo, M. (2018). Identification of a *S. aureus* virulence factor by activity-based protein profiling (ABPP). Nat. Chem. Biol. *14*, 609–617.

Li, H., and Durbin, R. (2009). Fast and accurate short read alignment with Burrows-Wheeler transform. Bioinformatics *25*, 1754–1760.

Li, M., Patel, H.V., Cognetta III, A.B., Smith II, T.C., Mallick, I., Cavalier, J.-F., Previti, M.L., Canaan, S., Aldridge, B.B., Cravatt, B.F., and Seeliger, J.C. (2021). Identification of cell wall synthesis inhibitors active against *Mycobacterium tuberculosis* by competitive activity-based protein profiling. Cell Chem. Biol. https://doi.org/10.1016/j.chembiol.2021.08.013.

Liu, Y., Patricelli, M.P., and Cravatt, B.F. (1999). Activity-based protein profiling: the serine hydrolases. Proc. Natl. Acad. Sci. U S A *96*, 14694–14699.

Low, K.L., Rao, P.S., Shui, G., Bendt, A.K., Pethe, K., Dick, T., and Wenk, M.R. (2009). Triacylglycerol utilization is required for regrowth of in vitro hypoxic nonreplicating *Mycobacterium bovis* bacillus Calmette-Guerin. J. Bacteriol. *191*, 5037–5043.

McEvoy, C.R., Cloete, R., Muller, B., Schurch, A.C., van Helden, P.D., Gagneux, S., Warren, R.M., and Gey van Pittius, N.C. (2012). Comparative analysis of *Mycobacterium tuberculosis* pe and ppe genes reveals high sequence variation and an apparent absence of selective constraints. PLoS One *7*, e30593.

Minnikin, D.E., Kremer, L., Dover, L.G., and Besra, G.S. (2002). The methyl-branched fortifications of *Mycobacterium tuberculosis*. Chem. Biol. *9*, 545–553.

Minnikin, D.E., Lee, O.Y., Wu, H.H., Besra, G.S., Bhatt, A., Nataraj, V., Rothschild, B.M., Spigelman, M., and Donoghue, H.D. (2015). Ancient mycobacterial lipids: key reference biomarkers in charting the evolution of tuberculosis. Tuberculosis (Edinb) *95 Suppl 1*, S133–S139.

Mohandas, P., Budell, W.C., Mueller, E., Au, A., Bythrow, G.V., and Quadri, L.E. (2016). Pleiotropic consequences of gene knockouts in the phthiocerol dimycocerosate and phenolic glycolipid biosynthetic gene cluster of the opportunistic human pathogen *Mycobacterium marinum*. FEMS Microbiol. Lett. *363*, fnw016.

Natarajan, V.T., Mohanty, D., and Gokhale, R.S. (2008). Biosynthesis of mycobacterial lipids by multifunctional polyketide synthases. In The Mycobacterial Cell Envelope, M. Daffé and J.-M. Reyrat, eds. (ASM Press), pp. 235–248. https://doi.org/10.1128/9781555815783.ch15.

Nguyen, P.C., Delorme, V., Benarouche, A., Martin, B.P., Paudel, R., Gnawali, G.R., Madani, A., Puppo, R., Landry, V., Kremer, L., et al. (2017). Cyclipostins and Cyclophostin analogs as promising compounds in the fight against tuberculosis. Sci. Rep. *7*, 11751.

Nguyen, P.C., Nguyen, V.S., Martin, B.P., Fourquet, P., Camoin, L., Spilling, C.D., Cavalier, J.F., Cambillau, C., and Canaan, S. (2018). Biochemical and structural characterization of TesA, a major thioesterase required for outer-envelope lipid biosynthesis in *Mycobacterium tuberculosis*. J. Mol. Biol. *430*, 5120–5136.

Onwueme, K.C., Vos, C.J., Zurita, J., Ferreras, J.A., and Quadri, L.E. (2005). The dimycocerosate ester polyketide virulence factors of mycobacteria. Prog. Lipid Res. *44*, 259–302.

Ortega, C., Anderson, L.N., Frando, A., Sadler, N.C., Brown, R.W., Smith, R.D., Wright, A.T., and Grundner, C. (2016). Systematic survey of serine hydrolase activity in *Mycobacterium tuberculosis* defines changes associated with persistence. Cell Chem. Biol. *23*, 290–298.

Patel, H.V., Li, M., and Seeliger, J.C. (2018). Opportunities and challenges in activity-based protein profiling of mycobacteria. Curr. Top Microbiol. Immunol. *420*, 49–72.

Patricelli, M.P., Giang, D.K., Stamp, L.M., and Burbaum, J.J. (2001). Direct visualization of serine hydrolase activities in complex proteomes using fluorescent active site-directed probes. Proteomics *1*, 1067–1071.

Ravindran, M.S., Rao, S.P.S., Cheng, X., Shukla, A., Cazenave-Gassiot, A., Yao, S.Q., and Wenk, M.R. (2014). Targeting lipid esterases in mycobacteria grown under different physiological conditions using activity-based profiling with tetrahydrolipstatin (THL). Mol. Cell Proteomics *13*, 435–448.

Rengarajan, J., Bloom, B.R., and Rubin, E.J. (2005). Genome-wide requirements for *Mycobacterium tuberculosis* adaptation and survival in macrophages. Proc. Natl. Acad. Sci. U S A *102*, 8327–8332.

Rens, C., Laval, F., Daffe, M., Denis, O., Frita, R., Baulard, A., Wattiez, R., Lefevre, P., and Fontaine, V. (2016). Effects of lipid-lowering drugs on vancomycin susceptibility of mycobacteria. Antimicrob. Agents Chemother. *60*, 6193–6199.

Santucci, P., Point, V., Poncin, I., Guy, A., Crauste, C., Serveau-Avesque, C., Galano, J.M., Spilling, C.D., Cavalier, J.F., and Canaan, S. (2018). LipG a bifunctional phospholipase/thioesterase involved in mycobacterial envelope remodeling. Biosci. Rep. *38*, BSR20181953.

Sassetti, C.M., Boyd, D.H., and Rubin, E.J. (2003). Genes required for mycobacterial growth defined by high density mutagenesis. Mol. Microbiol. *48*, 77–84.

Sassetti, C.M., and Rubin, E.J. (2003). Genetic requirements for mycobacterial survival during infection. Proc. Natl. Acad. Sci. U S A *100*, 12989–12994.

Seemann, T. (2015). Snippy: Fast Bacterial Variant Calling from NGS Reads, https://github.com/tseemann/snippy/blob/master/README.md.

Simon, G.M., and Cravatt, B.F. (2010). Activity-based proteomics of enzyme superfamilies: serine hydrolases as a case study. J. Biol. Chem. *285*, 11051–11055.

Tallman, K.R., Levine, S.R., and Beatty, K.E. (2016). Small-molecule probes reveal esterases with persistent activity in dormant and reactivating *Mycobacterium tuberculosis*. ACS Infect. Dis. *2*, 936–944.

Tautenhahn, R., Patti, G.J., Rinehart, D., and Siuzdak, G. (2012). XCMS Online: a web-based platform to process untargeted metabolomic data. Anal Chem. *84*, 5035–5039.

Trivedi, O.A., Arora, P., Vats, A., Ansari, M.Z., Tickoo, R., Sridharan, V., Mohanty, D., and Gokhale, R.S. (2005). Dissecting the mechanism and assembly of a complex virulence mycobacterial lipid. Mol. Cell *17*, 631–643.

Yang, D., Vandenbussche, G., Vertommen, D., Evrard, D., Abskharon, R., Cavalier, J.F., Berger, G., Canaan, S., Khan, M.S., Zeng, S., et al. (2020). Methyl arachidonyl fluorophosphonate inhibits *Mycobacterium tuberculosis* thioesterase TesA and globally affects vancomycin susceptibility. FEBS Lett. *594*, 79–93.

STAR★METHODS

KEY RESOURCES TABLE

REAGENT or RESOURCE	SOURCE	IDENTIFIER
Bacterial and virus strains		
Mycobacterium tuberculosis H37Rv	Carolyn Bertozzi (Stanford University)	N/A
Mycobacterium tuberculosis CDC1551	Carolyn Bertozzi (Stanford University)	N/A
Mycobacterium tuberculosis $mc^2$6020	Niaz Banaei (Stanford University)	N/A
Mycobacterium kansasii isolate	Nikki Parrish (Johns Hopkins University School of Medicine)	N/A
Mycobacterium scrofalaceum isolate	Nikki Parrish (Johns Hopkins University School of Medicine)	N/A
Mycobacterium intracellulare isolate	Nikki Parrish (Johns Hopkins University School of Medicine)	N/A
Mycobacterium abscessus isolate	Nikki Parrish (Johns Hopkins University School of Medicine)	N/A
Mycobacterium avium isolate	Nikki Parrish (Johns Hopkins University School of Medicine)	N/A
Mycobacterium marinum M	Carolyn Bertozzi (Stanford University)	N/A
Mycobacterium smegmatis $mc^2$155	Carolyn Bertozzi (Stanford University)	N/A
Escherichia coli MG1655	Coli Genetic Stock Center (Yale University)	Cat#6300
Staphylococcus aureus USA300	BEI Resources	Cat#USA300-0114
Chemicals, peptides, and recombinant proteins		
Recombinant *M. tuberculosis* TesA	This study	N/A
3,4-dichloroisocoumarin (DCI)	Millipore-Sigma	Cat#D7910
Lipase inhibitor, THL	Santa Cruz Biotechnology	Cat#sc-203108
FP-TMR	Bogyo laboratory stock (Liu et al., 1999)	N/A
FP-biotin	Bogyo laboratory stock (Patricelli et al., 2001)	N/A
JCP276	Bogyo laboratory stock (Kerrigan et al., 1995)	N/A
JCP275	Bogyo laboratory stock (Kerrigan et al., 1995)	N/A
BMB034	This study	N/A
BMB038	This study	N/A
Critical commercial assays		
CellTiter-Blue	Promega	Cat#G808B
Deposited data		
ABPP proteomics data	This study	https://doi.org/10.5061/dryad.41ns1rndp
Lipidomics data	This study	https://doi.org/10.5061/dryad.6q573n5zv
Experimental models: Cell lines		
HFF-1 human foreskin fibroblasts	ATCC	Cat#SCRC-1041
J774A.1 murine macrophages	Carolyn Bertozzi (Stanford University)	N/A
Oligonucleotides		
ppsA-seq.for, TCGACGCGGAATTCTTCGAG	This study	N/A
ppsA-seq.rev, AACCGCTTGAGCACCACTAC	This study	N/A
Recombinant DNA		
pET28b-His-TesA	This study	N/A

(*Continued on next page*)

Continued

REAGENT or RESOURCE	SOURCE	IDENTIFIER
Software and algorithms		
Prism version 9.1.0	GraphPad	https://www.graphpad.com
Python version 3.6.0	Python	https://www.python.org
Snippy	(Seemann, 2015)	https://github.com/tseemann/snippy
MaxQuant 1.6.1.0	(Cox and Mann, 2008)	https://www.maxquant.org
Lipidomic analysis code	This study	https://doi.org/10.5281/zenodo.4947639

RESOURCE AVAILABILITY

Lead contact

Further information and requests for resources and reagents should be directed to the lead contact, Matthew Bogyo (mbogyo@stanford.edu).

Materials availability

Plasmids and small molecules described in this study are available upon request.

Data and code availability

Proteomic data and lipidomics data have been deposited at Dryad and are publicly available as of the date of publication. All original code has been deposited at Zenodo and is publicly available. Accession numbers and DOIs for all datasets and code are listed in the key resources table. Any additional information required to reanalyze the data reported in this paper is available from the lead contact upon request.

EXPERIMENTAL MODEL AND SUBJECT DETAILS

Mycobacterial culture

Unless otherwise noted, *M. tuberculosis* was cultured in 7H9/OADC/glycerol medium (4.7 g/l 7H9 powder, 100 ml/l OADC supplement, 4 ml/l 50% (v/v) glycerol, and 2.5 ml/l 20% (v/v) TWEEN 80). OADC was made fresh before adding to the medium (0.5 g/l oleic acid, 50 g/l Albumin fraction V, 20 g/l dextrose, 40 mg/l catalase, and 8.5 g/l NaCl). Cultures were inoculated from 1 ml frozen bacterial stocks and incubated in 1 l roller bottles with rolling at 37°C for 1-2 weeks. *M. tuberculosis* solid cultures were grown on 7H10 medium (19 g/l 7H10 powder, 20 ml 50% (v/v) glycerol, 100 ml/l OADC supplement).

M. tuberculosis H37Rv, *Mycobacterium marinum* M, and *Mycobacterium smegmatis* mc^2155 were a gift from Carolyn Bertozzi (Stanford University). *M. tuberculosis* $mc^2$6020 was a gift from Niaz Banaei (Stanford University). The following clinical isolates of NTMs were a gift from Dr. Nikki Parrish and Derek Armstrong (Department of Pathology, the Johns Hopkins University School of Medicine): *Mycobacterium kansasii*, *Mycobacterium intracellulare*, *Mycobacterium scrofulaceum*, *Mycobacterium avium*, and *Mycobacterium abscessus*.

Bacterial culture for recombinant protein expression

E. coli BL21 (DE3) were grown in 2xYT medium to an OD_{600} of 0.4, induced with 1 mM IPTG, and allowed to express for 16 h at 20°C.

Mammalian cell culture

J774 murine macrophages and HFF-1 human foreskin fibroblasts were cultured in DMEM with 10% FBS at 37°C with 5% CO_2. Cell lines were not authenticated.

METHOD DETAILS

High-throughput screening, hit validation, and EC_{50} determination

The original screen was performed in 7H9/casitone/glucose medium (4.7 g/l 7H9 powder, 0.3 g/l casitone, 4 g/l glucose, 0.81 g/l NaCl, and 0.05% (v/v) tyloxapol). *M. tuberculosis* H37Rv was grown to OD_{600} of 0.6-0.7, diluted 500-fold into fresh medium, and 50 μl of the diluted culture were added to each well of 96 well-plates containing 50 μl of medium and test compound (final volume: 100 μl, final compound concentration: 20 μM, final DMSO concentration: 1% (v/v)). Each plate contained 8 wells of DMSO as a maximum growth control and 8 wells of 0.15 μM rifampicin as a minimum growth control. Plates were incubated without shaking for 6 d at 37°C, 10 μl alamarBlue was added to each well, the plate was incubated for an addition 1 d at 37°C, and viability in each well was scored visually.

Hits were validated by treating with ten-point dose response and estimating EC_{50} values. Growth inhibition was tested as above except cultures were grown in 7H9/OADC/glycerol medium and CellTiterBlue (Promega) was used as a measure of cell viability.

Viability was quantified by fluorescent measurement (Ex. 560 nm, Em. 590 nm) in a SpectraMax M3 microplate reader (Molecular Devices). For validation experiments, each compound was tested in a single replicate. For JCP276, BMB034, and BMB038, each compound was tested in biological triplicate. Fluorescence values were normalized to DMSO (100% viability) and 150 nM rifampicin (0% viability). Data were fit to a two-parameter logistic model to calculate EC_{50} values.

Growth inhibition measurements

M. tuberculosis H37Rv was diluted to OD_{600} of 0.001 and 5 ml of culture was aliquoted into ink well bottles. Cultures were treated with DMSO, 25 μM JCP276 on day 0, or 25 μM on day 0 and an additional 25 μM on day 14. Cultures were grown with shaking at 37°C for up to 6 weeks. Growth was monitored by transferring cultures to a 96-well plate and measuring OD_{600} in a SpectraMax M3 microplate reader (Molecular Devices). The experiment was performed in biological triplicate.

MIC measurements

M. tuberculosis strains H37Rv and CDC1551, *M. marinum strain* M, *M. smegmatis* strain mc^2155, and clinical isolates of *M. kansasii, M. scrofulaceum, M. intracellulare, M. abscessus,* and *M. avium* were cultured in 7H9/OADC/glycerol medium. *M. tuberculosis* mc^26020 was cultured in 7H9/OADC/glycerol medium supplemented with pantothenate (24 mg/l), L-lysine (80 mg/l), and 0.2% (w/v) casamino acids. *Escherichia coli* strain MG1655 and *Staphylococcus aureus* strain USA300 were cultured in Mueller-Hinton II broth. *M. marinum* was cultured at 33°C and all other bacteria were cultured at 37°C.

Cultures were diluted to OD_{600} 0.001 and 100 μl of each diluted culture was added to 96 well-plates containing JCP276 at various doses (100 nM to 100 μM) and DMSO control wells. Plates were incubated and scored visually for dense bacterial growth. *M. tuberculosis* strains were scored after 3 weeks. All other bacteria were scored after 1 d to 2 weeks after dense growth was observed in the DMSO control wells. MICs were determined as the lowest dose that prevented bacterial growth in all three biological replicates.

Mammalian cell cytotoxicity measurements

Cells were seeded into 96-well plates (20,000 cells/well) and incubated for 1 d. Cells were washed with PBS and resuspended in serum-free DMEM containing DMSO or various concentrations of JCP276 (1% maximum DMSO concentration). Plates were incubated for 24 h and viability was measured following a 6 h incubation with CellTiterBlue (Promega). Viability was quantified by fluorescent measurement (Ex. 560 nm, Em. 590 nm) in a Cytation 3 microplate reader (Biotek). Fluorescence values were normalized to DMSO (100% viability) and wells containing no cells (0% viability). The experiment was performed in biological triplicate.

Compound stability measurements

JCP276 (100 μM) was added to 7H9/OADC medium and incubated at 37°C for up to 7 days. Aliquots were removed and added to acetonitrile (1:4 medium:acetonitrile) to precipitate protein. Samples were centrifuged at 15,000 kg for 2 min. Supernatants were analyzed by LC-MS. JCP276 was quantified by integrating the absorbance peak at 355 nm. No peak was observed in the absence of compound. Peak areas were normalized to the peak area before incubation (time 0). The half-life was calculated by fitting normalized peak areas to an exponential decay curve (n=2).

Generation of resistant mutants

M. tuberculosis H37Rv (BBMT01) was grown to an OD_{600} of 1, centrifuged, and concentrated 10-fold ($\sim 10^9$ CFU/ml). Concentrated cultures (1 ml) were added to 7H10 solid medium containing 100 μM JCP276 and allowed to incubate for 3 weeks. Bacteria grown in the presence of JCP276 from three separate plates were used to start liquid cultures which were then tested for JCP276 susceptibility and frozen for future use (annotated BBMT04, BBMT05, and BBMT06).

Whole genome and sanger sequencing of mutants

Cultures of BBMT01, BBMT04, BBMT05, and BBMT06 were grown in liquid culture to an OD_{600} of 1. Cultures were centrifuged and resuspended in breaking buffer (50 mM Tris pH 8, 10 mM EDTA, and 100 mM NaCl). Bacteria were lysed by bead beating, the supernatant was transferred to a clean O-ring tube, and the samples were adjusted to 1% final concentration of SDS. Samples were filtered through 0.22 μm syringe filters twice and removed from the BSL3 facility. DNA was purified using a Qiagen cleanup kit.

DNA sequencing libraries were prepared using the Illumina DNA Prep kit (formerly named Nextera DNA Flex kit; Illumina, San Diego, CA, USA). AMPure XP beads (Beckman Coulter, San Jose, CA, USA) were substituted in place of Sample Purification Beads (SPB) in the library clean up steps of the protocol. Library concentration was measured using the Qubit 3.0 Fluorometric Quantitation dsDNA High Sensitivity kit (ThermoFisher Scientific, Waltham, MA, USA). Library size distribution was analyzed with the High Sensitivity DNA Chip and reagent kit on the Bioanalyzer 2100 (Agilent, Santa Clara, CA). Libraries were multiplexed using IDT for Illumina Nextera DNA Unique Dual Indexes Set C. Library quality control and subsequent sequencing was performed by Novogene Co. using 150 base pair paired-end reads generated on the NovaSeq 6000 platform (Illumina, San Diego, CA, USA).

	BBMT01	BBMT05
DNA concentration	40.0 ng/μl	28.0 ng/μl
UD indices used	GCGTGGATGG, CATTGGTCAA	TCCTGGTTGT, TGCCGGTCAG
Library concentration	10.5 ng/μl	5.42 ng/μl
Library size distribution peak	~500 bp	~500 bp

For confirmation of the *ppsA* mutation, the region of interest was amplified by PCR using primers *ppsA-seq.for* and *ppsA-seq.rev* and analyzed by Sanger sequencing.

Variant calling

The reference genome of the *M. tuberculosis* H37Rv was downloaded from NCBI (accession: NC_000962.3). Variant calling, between sample reads and the H37Rv reference genome, was performed using the haploid variant calling pipeline Snippy (version 4.6.0) with default parameters. Briefly, reads were mapped to the reference genome using BWA MEM (Li and Durbin, 2009) and variants were called using freebayes (Garrison and Marth, 2012). Intersected/complement variants between the wild-type and mutant samples were calculated using bcftools isec (Danecek et al., 2021).

PDIM analysis by TLC

Cultures of *M. tuberculosis* or NTM strains were grown to an OD_{600} of ~1. Cells were pelleted by centrifugation and resuspended in PBS to an OD_{600} of 10. Cells were killed by incubating at 95°C for 1 h. Cell pellets were dried by lyophilization and lipids were extracted three times with 2 ml of petroleum ether. Extracted lipids were dried and resuspended in DCM at a concentration of 2 mg/ml. Lipid samples were loaded onto silica TLC plates and separated by a mobile phase of 97:3 petroleum ether:ethyl acetate. Plates were dried, sprayed with 10% (w/v) $CuSO_4$ in 1.3 M phosphoric acid, and developed by heating. The PDIM standard was extracted from *M. marinum* and kindly provided by CJ Cambier (Stanford University).

ABPP labeling and enrichment

Cultures of *M. tuberculosis* H37Rv were centrifuged and resuspended to a final OD_{600} of 2.5 in 7H9 buffer (4.7 g/l). Cultures were treated with JCP275, or JCP276, or DCI and incubated at 37°C for 1 h. For FP labeling, cells were lysed (see below) and lysates were treated with 1 μM FP-TMR or 5 μM FP-biotin for 30 min at 37°C. For BMB034 labeling, cells were treated with BMB034 for 1 h at 37°C immediately after compound treatment and then lysed.

Bacteria were resuspended in PBS and lysed by bead beating at room temperature. Triton-X was added to a final concentration of 1% and lysates were clarified by centrifugation at 2800 rcf for 5 min at room temperature. Lysates were filtered twice through 0.2 μm syringe filters for removal from the BSL3 facility.

For FP-TMR experiments, lysates were analyzed directly by SDS-PAGE. For BMB034 experiments, lysates were subjected to click chemistry conditions (5 mM BTTAA, 1mM $CuSO_4$, and 15 mM sodium ascorbate) with 20 μM azide-TMR for 30 min at 37°C and analyzed by SDS-PAGE. For BMB034 enrichments, lysates were subjected to click chemistry conditions with 20 μM desthiobiotion-TMR-azide for 1 h at 37°C.

Biotinylated protein samples were desalted using PD-10 columns. Proteins were eluted into PBS and SDS was added to a final concentration of 0.05%. Samples were heated at 90°C for 8 min and then cooled at -20°C for 5 min. Streptavidin-agarose was washed in PBS and 100 μl of slurry was added to each protein sample and allowed to mix for 1 h at room temperature. Agarose resin was pelleted by centrifugation at 4000 rcf for 5 min between each of the following washes: twice with 1% SDS, twice with 6 M urea, and twice with PBS. Beads were aspirated and then resuspended in 500 μl 6 M urea. Proteins were reduced by addition of 25 μl of 30 mg/ml DTT and incubation for 15 min at 65°C. Samples were cooled and proteins were alkylated by addition of 25 μl of 14 mg/ml iodoacetamide and incubation for 30 min at 37°C. Beads were rinsed once with 1 ml PBS and resuspended in digestion buffer (200 μl 2 M urea, 2 μl 1 M $CaCl_2$, 4 μl of 0.5 mg/ml trypsin). Proteins were digested for 16 h at 37°C.

Beads were transferred to spin filters and washed twice with 50 μl PBS to yield digested peptides. Peptides were acidified by addition of 15 μl formic acid and desalted using C18 zip tips. Peptides were eluted into 75% acetonitrile with 1% formic acid, dried, and stored at -20°C for subsequent LC-MS/MS analysis.

Proteomic analysis

Peptides were resuspended in 0.2% formic acid in water. Peptides were separated over a 25-cm EasySpray reversed phase LC column (75 μm inner diameter packed with 2 μm, 100 Å, PepMap C18 particles, Thermo Fisher Scientific). The mobile phases (A: water with 0.2% formic acid and B: acetonitrile with 0.2% formic acid) were driven and controlled by a Dionex Ultimate 3000 RPLC nano system (Thermo Fisher Scientific). Gradient elution was performed at 300 nl min^{-1}. For the FP ABPP experiment, the mobile phase was ramped to 3% B over 3 min, followed by a ramp to 35% B at 93 min, a ramp to 42% B at 103 min, and a wash at 95% B for 10 min. For the BMB034 ABPP experiment, the mobile phase was ramped to 5% B over 4 min, followed by a ramp to 25% B at 72 min, and a wash at 9% B for 6 min. Eluted peptides were analyzed on an Orbitrap Fusion Tribrid MS system (Thermo Fisher Scientific). Survey

scans of peptide precursors were collected in the Orbitrap from 300-1500 m/z for the FP ABPP experiment or 350-1350 m/z for the BMB034 ABPP experiment. Monoisotopic precursor selection was enabled for peptide isotopic distributions, precursors of z = 2–5 were selected for data-dependent MS/MS scans for 2 s of cycle time.

Proteomic data analysis

Raw data files were analyzed using MaxQuant (v. 1.6.1.0) with the following parameters: trypsin digestion with maximum of 2 missed cleavages, variable modifications of oxidized methionine residues and acetylated N-termini, fixed modifications of carbamidomethylation at cysteine residues, peptide tolerance of 4.5 ppm, and a FDR of 1%. Peptides were quantified using LFQ with a minimum peptide count of 2, MS/MS of at least one peptide required for quantification, and using re-quantification and matches between runs. Data were searched against the reference H37Rv proteome. FP and BMB034 enrichment experiments were analyzed separately and results were merged (Table S4). Protein abundance ratios were calculated by dividing LFQ values from compound-treated samples by those from DMSO-treated samples. In cases where proteins were not identified in compound-treated samples, $\log_2$ ratios were arbitrarily set to -10.

Lipid extraction

M. tuberculosis H37Rv liquid cultures at OD_{600} of 1 were transferred to 0.22 μm membranes placed on 7H10 solid medium and incubated for 1 week at 37°C to yield a lawn of bacteria on each membrane. Membranes were transferred to 6-well plates containing 7H10 solid medium with 1% DMSO, 100 μM JCP276, 100 μM BMB034, or 100 μM THL. Membranes were incubated for 24 h at 37°C. Each membrane was transferred to an O-ring tube and lipids were extracted form whole cells by vortexing once each with 0.5 ml 1:2 chloroform:methanol, 0.5 ml 1:1 chloroform:methanol, and 0.5 ml 2:1 chloroform:methanol. Supernatants from the three extractions were combined and filtered twice through 0.22 μm syringe filters before removal from the BSL3 facility. Extracts were transferred to glass vials and solvent was dried under nitrogen gas. Samples were dried completely by rotary evaporation. The dry mass of each lipid sample was measured and lipids were resuspended in 2:1 chloroform:methanol to a final concentration of 5 mg/ml.

Lipidomic analysis

Mass spectrometry analysis was performed with an electrospray ionization source on an Agilent 6520 Q-TOF LC/MS in negative ionization mode. For Q-TOF acquisition parameters, the mass range was set from 100 to 1700 m/z with an acquisition rate of 1 spectra/second and time of 1000 ms/spectrum. For Dual AJS ESI source parameters, the drying gas temperature was set to 250°C with a flow rate of 12 l/min, and the nebulizer pressure was 20 psi. The capillary voltage was set to 3500 V and the fragmentor voltage was set to 100 V. Reversed-phase chromatography was performed with a Luna 5 mm C5 100 Å LC column (Phenomenex cat #00B-4043-E0). Samples were injected at 20 ul each. Mobile phases for were as follows: Buffer A, 95:5 water/methanol with 0.1% ammonium hydroxide; Buffer B, 60:35:5 isopropanol/methanol/water with 0.1% ammonium hydroxide. All solvents were HPLC-grade. The flow rate for each run started with 0.5 minutes 95% A / 5% B at 0.6 ml/min, followed by a gradient starting at 95% A / 5% B changing linearly to 5% A / 95% B at 0.6 ml/min over the course of 19.5 minutes, followed by a hold at 5% A / 95% B at 0.6 ml/min for 8 minutes and a final 2 minute at 95% A / 5% B at 0.6 ml/min.

Lipidomic data analysis

Raw files were converted to mzXML format with MSConvert (ProteoWizard) using the Peak Picking Vendor algorithm. Files were analyzed using the web-based XCMS platform (Tautenhahn et al., 2012) with the following settings: signal to noise threshold, 6; maximum tolerated m/z deviation, 30 ppm; frame width for overlapping peaks, 0.01; and peak width, 10-60 s. Integrated peak intensities were normalized between conditions by median fold change. Tables containing mass features and ion intensities from each experiment were downloaded from the XCMS platform. Identified ions were matched to the MycoMass database (Layre et al., 2011) using a custom python script. Ions were matched if the measured m/z was within 10 ppm of the annotated m/z.

Analysis of SH homologs

The protein sequence of SHs from *M. tuberculosis* H37Rv were used as the query sequence for BLASTP analysis. The search set comprised whole proteome sequences from *M. kansasii* strain ATCC 12478, *M. marinum* strain M, *M. scrofulaceum* strain ASM208673v1, *M. avium subsp. hominissuis*, *M. intracellurale* strain ATCC 13950, *M. abscessus* strain ASM160629v1, *M. smegmatis* strain mc^2155, and the human proteome. Each SH was queried against the protein sequences by BLASTP (2.9.0+), requiring a minimum e-value of 10^{-30}.

Purification and FP competition of recombinant TesA

The *tesA* gene was amplified by PCR from chromosomal H37Rv DNA and cloned into pET28b to generate pET28b-TesA, encoding a 6xHis tag on the N-terminus of the protein. The expression vector was transformed into *E. coli* BL21/DE3.

Following expression, cultures were centrifuged and the combined pellet was lysed by sonication in lysis buffer (50 mM NaH_2PO_4 pH 7.5, 300 mM NaCl, 5 mM imidazole). The lysate was clarified by centrifugation and the soluble protein was purified on a HisTrap column on an Akta chromatography system, using gradient elution from 100% lysis buffer to 100% elution buffer (50 mM NaH_2PO_4 pH 7.5, 300 mM NaCl, 300 mM imidazole). Fractions containing TesA, as confirmed by SDS-PAGE, were combined and further purified by gel filtration with a Superdex 75 column using GF buffer (50 mM NaH_2PO_4 pH 7.5, 100 mM NaCl).

Purified TesA (100 nM) was incubated with DMSO or various concentrations of JCP276 for 30 min at 4°C and was then treated with 1 μM FP-TMR for 15 min at 4°C. The sample was immediately quenched by addition of SDS buffer and separated by SDS-PAGE.

Chemical synthesis

FP-TMR and FP-biotin were synthesized as previously described (Liu et al., 1999; Patricelli et al., 2001). JCP276 was synthesized as previously described (Kerrigan et al., 1995). Chemicals were purchased from Millipore Sigma.

BMB034 [1-(3-(but-3-yn-1-yloxy)-4-chloro-1-oxo-1H-isochromen-7-yl)-3-phenylurea]

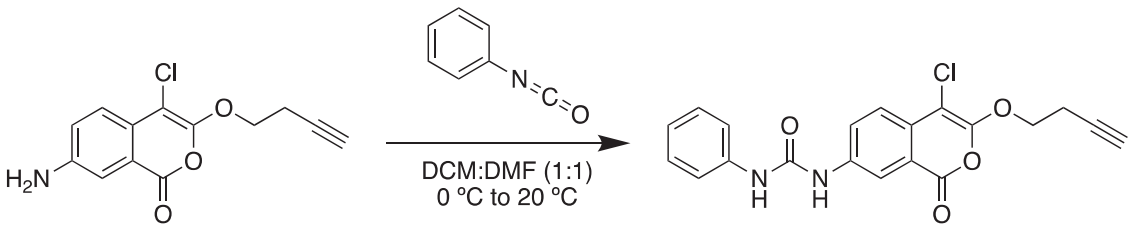

CLH130a BMB034

CLH130a was synthesized as previously described (Haedke et al., 2012). CLH130a (10mg, 0.038 mmol) was dissolved in 400 μl DCM:DMF (1:1) at 0°C. Phenyl isocyanate (4.98 mg, 0.042 mmol) was added dropwise to the flask over the course of 20 min and then allowed to warm to 20°C and react for 4 h. The solvent was removed by rotary evaporation and the reaction mixture was dissolved in ethyl acetate, washed with water and brine, and dried with magnesium sulfate. The mixture was purified by reverse phase chromatography and lyophilized to yield the final product (3.5 mg, 0.0091 mmol, 24% yield).

^{1}H NMR (400 MHz, DMSO-d6) δ 9.37 (s, 1H), 9.00 (s, 1H), 8.41 (d, J = 2.0 Hz, 1H), 7.87 (d, J = 8.7 Hz, 1H), 7.65 (d, J = 8.6 Hz, 1H), 7.48 (d, J = 7.9 Hz, 2H), 7.29 (t, J = 7.7 Hz, 2H), 6.99 (t, J = 7.4 Hz, 1H), 4.40 (t, J = 6.3 Hz, 2H), 2.95 – 2.90 (m, 1H), 2.73 – 2.66 (m, 2H); LRMS (ESI+) *m/z:* 383.1 $[M + H]^+$.

BMB038 [1-(3-(3-bromopropoxy)-4-chloro-1-oxo-1H-isochromen-7-yl)-3-(4-ethynylphenyl)urea]

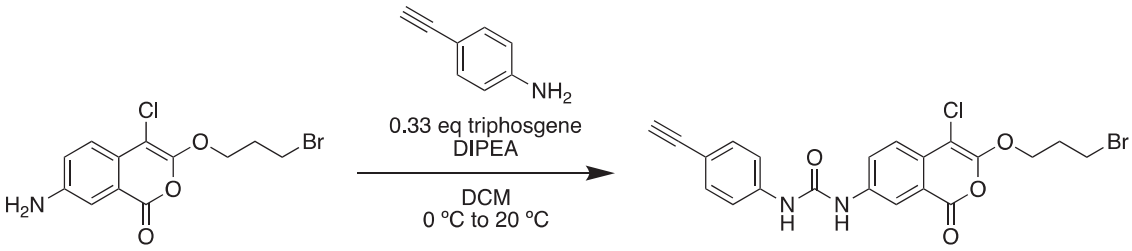

BMB037 BMB038

BMB037 was synthesized as previously described (Kerrigan et al., 1995). Triphosgene (3.0 mg, 0.01 mmol) was added to 100 μl DCM at 0°C. BMB037 (10 mg, 0.03 mmol) and diisopropylethylamine (10.5 μl, 0.06 mmol) were combined in 200 μl DCM at 0°C. This mixture was added dropwise to the triphosgene with stirring over the course of 20 min at 20°C. 4-ethynylaniline (3.9 mg, 0.033 mmol) and diisopropylethylamine (21 μl, 0.12 mmol) were combined in 200 μl DCM and were added at once to the reaction mixture. The reaction was allowed to proceed for 4 h at 20°C. The solvent was removed by rotary evaporation and the reaction mixture was dissolved in ethyl acetate, washed with potassium bisulfate, 5% sodium bicarbonate, and brine, dried with magnesium sulfate. The mixture was purified by silica chromatography (gradient from 10% to 30% ethyl acetate in hexanes) to yield the final product (3.3 mg, 0.069 mmol, 23% yield).

^{1}H NMR (400 MHz, DMSO-d6) δ 9.27 (s, 1H), 9.08 (s, 1H), 8.40 (d, J = 2.4 Hz, 1H), 7.88 (dd, J = 8.7, 2.4 Hz, 1H), 7.66 (d, J = 8.7 Hz, 1H), 7.53 – 7.49 (m, 2H), 7.43 – 7.40 (m, 2H), 4.51 – 4.39 (m, 2H), 3.69 (t, J = 6.5 Hz, 2H), 2.30 (q, J = 6.4 Hz, 3H); LRMS (ESI+) *m/z:* 475.0 $[M + H]^+$.

QUANTIFICATION AND STATISTICAL ANALYSIS

Plotting and statistical analysis were performed with Prism (GraphPad, v. 9.1.0) or python (v. 3.6.0) with numpy (v. 1.17.4), scipy (v. 1.3.2), matplotlib (3.0.3), and seaborn (v. 0.9.0) packages. Proteomics data were analyzed using MaxQuant. Lipidomics data were analyzed using msConvert and the online XCMS platform (Gowda et al., 2014).

Statistical details for each experiment are described in the figure legends. The number of biological replicates performed using independent bacterial or cell cultures (n) are given for each experiment. Plots show the mean and standard deviation of replicate measurements unless otherwise noted. For proteomic analyses, p-values were adjusted for multiple hypothesis testing using the Benjamini-Hochberg procedure. Null hypotheses were rejected for p-values or adjusted p-values < 0.05.